Applying Massively Parallel Interface for MPFA scheme with advanced linearization for fluid flow in porous media

Li, Longlong; Khait, Mark; Voskov, Denis; Terekhov, Kirill M.; Abushaikha, Ahmad

DOI
10.1016/j.petrol.2022.111190

Publication date
2023

Document Version
Final published version

Published in
Journal of Petroleum Science and Engineering

Journal of Petroleum Science and Engineering 220 (2023) 111190

Contents lists available at ScienceDirect

Journal of Petroleum Science and Engineering

journal homepage: www.elsevier.com/locate/petrol

Applying Massively Parallel Interface for MPFA scheme with advanced linearization for fluid flow in porous media

Longlong Li [a,b,*], Mark Khait [c], Denis Voskov [c,d], Kirill M. Terekhov [e], Ahmad Abushaikha [b,**]

[a] Institute of Mechanics, Chinese Academy of Sciences, Beijing, China
[b] College of Science and Engineering, Hamad Bin Khalifa University, Education City, Qatar Foundation, Doha, Qatar
[c] Delft University of Technology, Department of Geoscience & Engineering, Stevinweg 1, 2628 CN, Delft, Netherlands
[d] Department of Energy, Science and Engineering, School of Earth Sciences, Stanford University, 367 Panama Street, 065 Stanford, CA 94305, USA
[e] Marchuk Institute of Numerical Mathematics, Russian Academy of Sciences, Gubkin Str., 8, Moscow, 119333, Russia

ARTICLE INFO

Keywords:
Reservoir simulation
Parallel framework
Multipoint flux approximation
Operator-based linearization
Unstructured grid
Full tensor permeability

ABSTRACT

We apply Massively Parallel Interface for MPFA-O scheme with state-of-the-art Operator-Based Linearization (OBL) approach for multiphase flow in porous media. The implementation of MPFA-O scheme enhances the modelling capabilities for non-**K**-orthogonal mesh. A fully implicit scheme is applied to guarantee the stability of solutions when a mass-based formulation is involved to keep the flexibility of the framework for general-purpose reservoir simulation. As the MPFA-O introduces more non-zeros elements in the Jacobian matrix than the traditional TPFA, massively parallel computations via Message Passing Interface (MPI) in this work help to guarantee competitive computational efficiency for high-fidelity geological models. Concerning the Jacobian assembly hassle, we apply the OBL approach which introduces operators combining the fluid and rock properties in the conservation equations and discretizes the operators in the physical parameter space. By computing values and derivatives of the operators via a multilinear interpolation, the assembly of Jacobian matrix and residual vector could be drastically simplified. Another benefit of the OBL is that by only evaluating operator values on the predefined nodes in the physical parameter space, the overhead related to complex phase behavior and property evaluation is significantly reduced. In the end, we present several benchmark cases to rigorously demonstrate the accuracy, convergence, and robustness of the framework and two challenging field-scale cases to further prove its computing performance and parallel scalability.

1. Introduction

Characterization of the geological model is of vital importance for oil and gas field management. An accurate reservoir characterization model (RCM) could provide intensified assistance to low-cost and risk-controlled decision making in practical projects. However, it is always challenging to construct a geological formation accurately due to the uncertainties in the subsurface characterization and strong heterogeneities including faults, fractures, and pinchouts. To deal with that, the reservoir simulation technology which is the most efficient and best solution is usually applied to quantify the geological features through inverse modelling. In this approach, the simulation accuracy and the simulation efficiency which determines the number of iterations in limited time have a great influence on the finally adopted geological model. Therefore, a powerful reservoir simulator that is accurate and efficient is quite important in RCM. Moreover, the performance of the simulator plays a significant role in the optimization process of development strategies as well.

Mathematically, the reservoir simulation is supposed to solve a nonlinear system of coupled conservation equations and constitutive relations. The nonlinearity of the system is mainly introduced by the complex grid geometry in RCM, complicated phase behavior, and non-uniform formation properties. To tackle the challenges associated with these complexities, researchers exert a lot of effort to design optimal discretization schemes in space and time, nonlinear solvers, linear solvers, and phase behavior computations.

The spatial discretization helps to approximate the fluxes through faces connecting grid blocks. For the purpose of different applications,

* Corresponding author. Institute of Mechanics, Chinese Academy of Sciences, Beijing, China.
** Corresponding author.
E-mail addresses: lilonglong@imech.ac.cn (L. Li), aabushaikha@hbku.edu.qa (A. Abushaikha).

https://doi.org/10.1016/j.petrol.2022.111190
Received 21 August 2021; Received in revised form 12 September 2022; Accepted 30 October 2022
Available online 9 November 2022

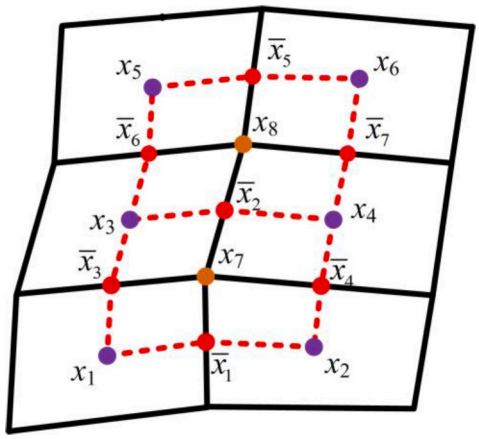

Fig. 1. The schematic of control volumes and intersection volumes.

many schemes have been proposed. Among all the schemes, the two-point flux approximation (TPFA) is widely used in many reservoir simulation softwares because of its simplicity. However, it requires **K**-orthogonal mesh of which the grid is structured and aligned with the principal directions of the permeability (Aziz and Settari, 1979). Owing to the inconsistency on non-**K**-orthogonal mesh (Settari and Aziz, 1972), it fails to provide convergent solutions for the simulation of complex geological models having an unstructured grid and full tensor permeability.

To tackle the challenges in TPFA, the multipoint flux approximation (MPFA) is proposed in (Aavatsmark et al., 1994, 1996a, 1996b, 1998; Edwards and Rogers, 1994, 1998) to provide correct spatial discretizations for non-**K**-orthogonal mesh. Having advantages for the cases with unstructured mesh and full tensor permeability, the MPFA is further extended in (Faille, 1992; Nordbotten and Eigestad, 2005; Wheeler and Yotov, 2006; Contreras et al., 2019; Cao et al., 2009). In addition, the extensive discussions in (Wheeler and Yotov, 2006; Klausen and Winther, 2006a, 2006b; Aavatsmark et al., 2006, 2007a, 2007b, 2008; Forsyth and Sammon, 1988; Njifenjou and Nguena, 2006; Aavatsmark and Eigestad, 2006; Eigestad and Klausen, 2005; Pal et al., 2006) prove the convergence of this scheme and indicate the prospective applications in reservoir simulation. Among all the MPFA versions, the O method is the classical and most intuitive method applicable for general applications (Aavatsmark, 2007). Futhermore, monotone nonlinear finite-volume methods that are robust and preserving are proposed (Schneider et al., 2018; Gao and Wu, 2013).

Apart from the control volume methods, the finite element method has also been improved to tackle the challenges (Brezzi and Fortin, 1991; Abushaikha et al., 2015, 2017; Moshiri and Manzari, 2019;

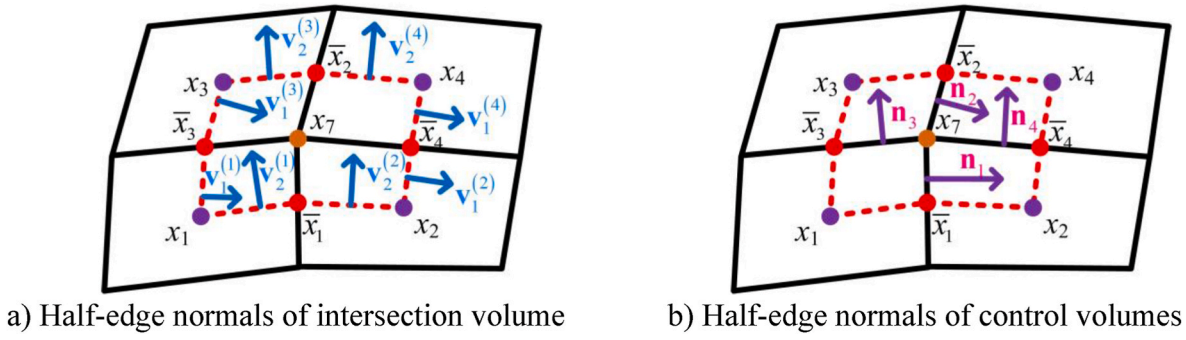

Fig. 2. Normal vectors inside an interaction volume.

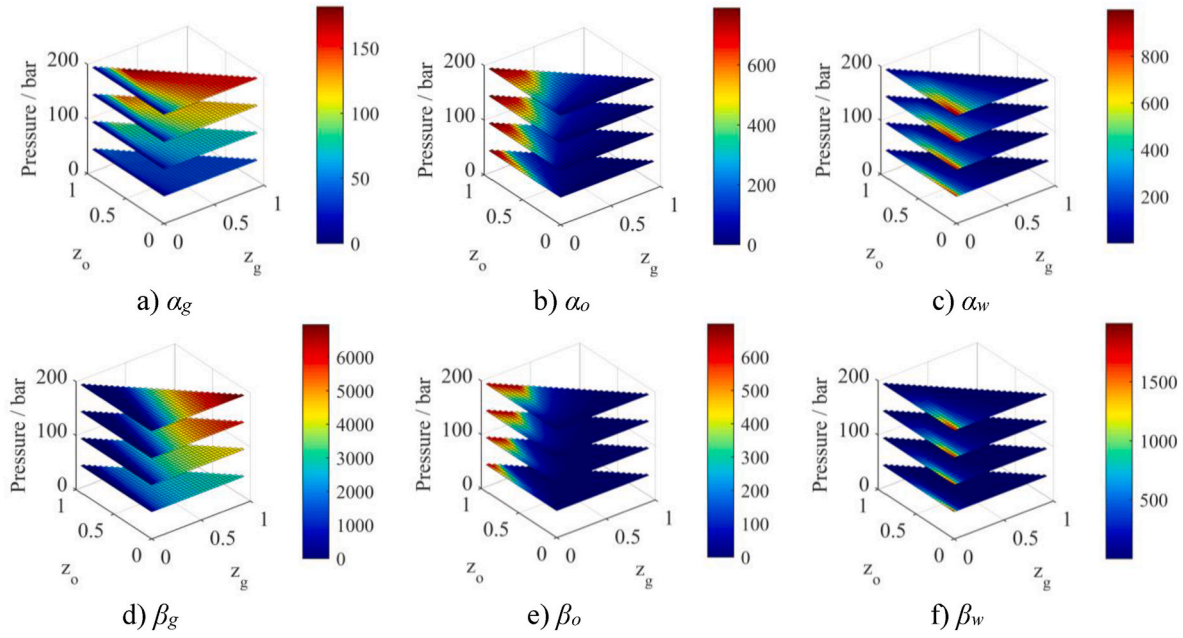

Fig. 3. An intuitive representation of the operators in a black oil system (OBL resolution is 32).

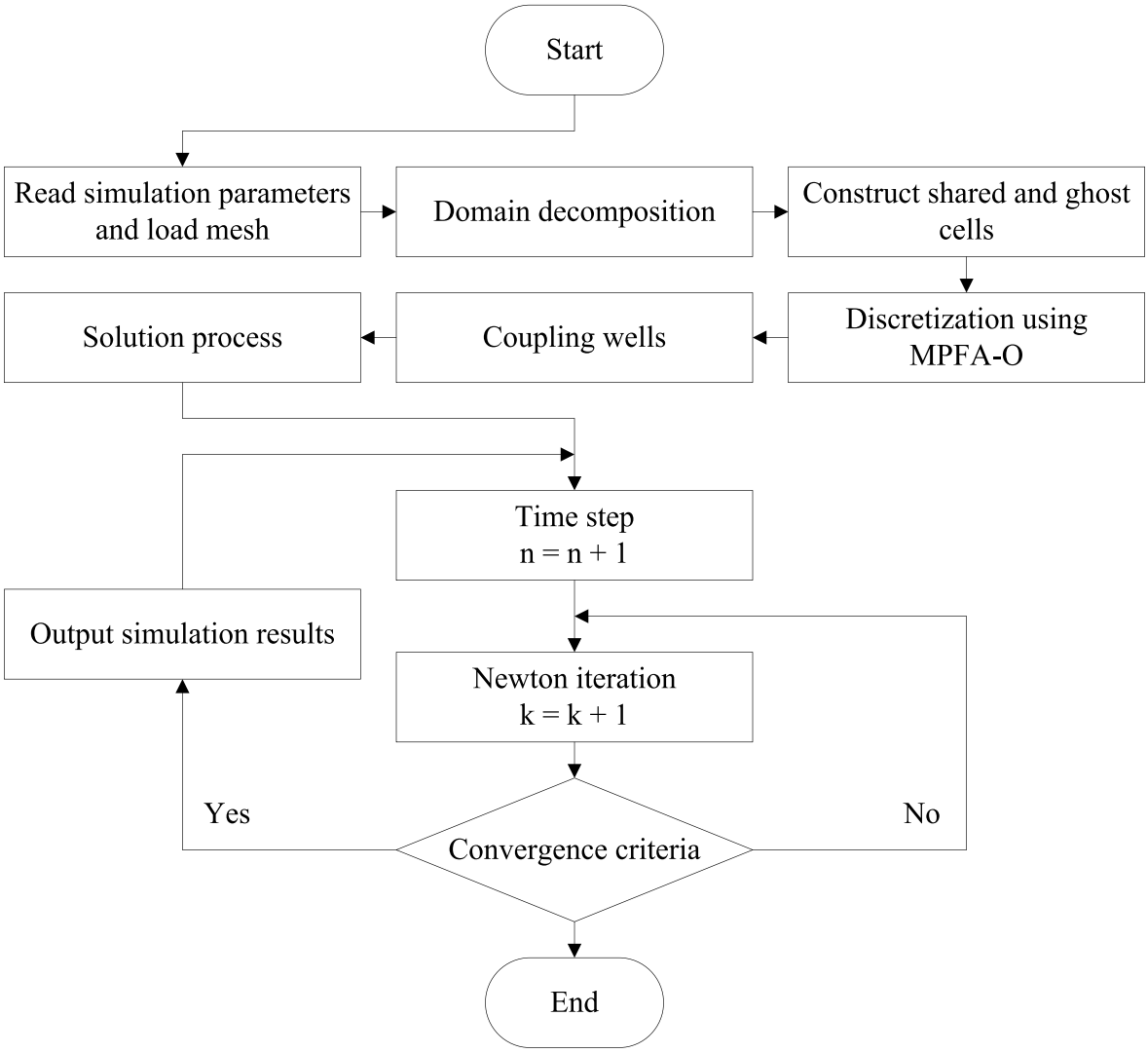

Fig. 4. The flowchart for implementation work.

Younes and Fontaine, 2008; Moortgat and Firoozabadi, 2016; Arrarás and Portero, 2019). In the variously derived versions, the mixed-finite-element method (MFEM), which solves the coupled conservation and momentum equations simultaneously, is locally conservative and is capable to handle the anisotropic properties (Brezzi and Fortin, 1991). However, it leads to a saddle-point problem. To address this issue, the mixed-hybrid finite-element (MHFE) method is proposed and applied in reservoir simulation (Moshiri and Manzari, 2019; Younes and Fontaine, 2008; Moortgat and Firoozabadi, 2016; Arrarás and Portero, 2019; Abushaikha et al., 2017). The mimetic finite difference scheme (MFD), part of the MHFE family, is presented to handle any shape of polygonal and polyhedral meshes (Tikhonov and Samarskii, 1962; Lipnikov et al., 2014). Holding the advantages of MFEM and the flexibility on a general mesh, the application of MFD in reservoir simulation gains some success (Zhang et al., 2017; Alpak, 2010; Lie et al., 2012; Abushaikha and Terekhov, 2020). But unfortunately, the unknowns on the interfaces bring more challenges for linear solver compared with the TPFA and MPFA methods.

Important as the spatial discretization is, the discretization scheme in time also plays a vital role in reservoir simulation. Generally, the discretization scheme in time can be classified into several types including fully implicit, adaptive implicit, and implicit pressure explicit saturation (Li et al., 2004). Among them, the fully implicit scheme is the most robust in that it avoids numerical limitations such as the CFL limit. For that reason, this scheme is widely used to solve multiple simulation models in many reservoir simulation softwares. However, the application of this scheme may bring severe nonlinearity to the system. Aimed to provide efficient solutions, several types of selections of nonlinear unknowns have been proposed. As summed up in (Voskov, 2017), the types, also called as formulations can be classified into two classes including mass-based and phase-based formulations. Usually, the mass-based formulation has less nonlinear unknown variables than the phase-based formulation. Although this simplifies the linear solution, more phase behavior calculations are required for the assembly of Jacobian matrix and residual vector in the mass-based formulation. Therefore, the phase-based formulation can be more efficient in comparison to the mass-based formulation in the field applications having complex phase behavior.

Apart from selection of the formulation, the linearization of the system at each nonlinear iteration is also quite important for the fully implicit scheme. In this process, it is always challenging to determine the value and derivatives of the properties and involve them in the Jacobian matrix and residual vector. Traditionally, there are three ways to deal with that including the numerical approach, straightforward hand-differentiation approach, and automatic differentiation techniques. The numerical approach is quite flexible but often fails to offer a robust solution. What important is that it can be expensive for multicomponent systems (Pruess et al., 1999; Pruess, 2004). The straightforward hand-differentiation approach is the most accurate strategy and has

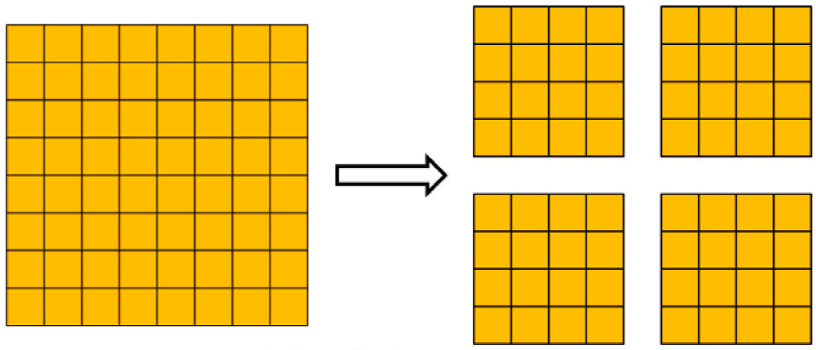

a) domain decomposition

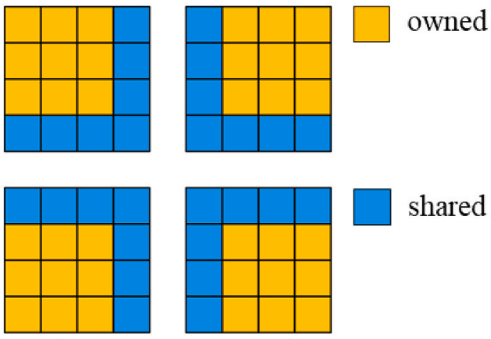

b) determine shared cells

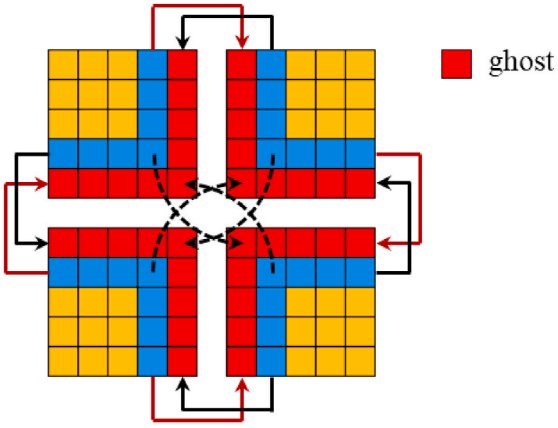

c) construct ghost cells (MPFA-O)

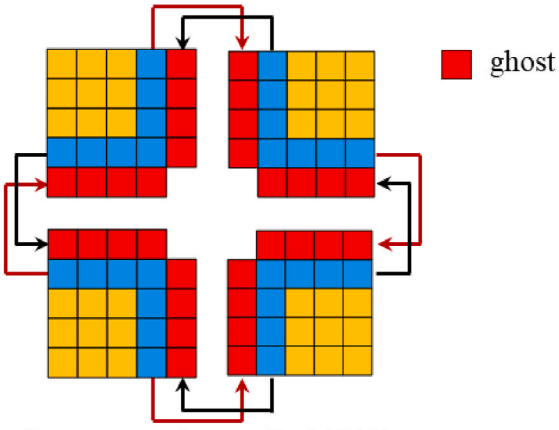

d) construct ghost cells (TPFA)

Fig. 5. The grids for parallel simulation. Owned grid in yellow, shared cell in blue, ghost cell in red. (For interpretation of the references to color in this figure legend, the reader is referred to the Web version of this article.)

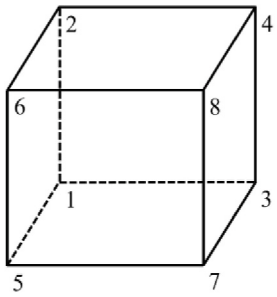

Fig. 6. Hexahedral grid.

Table 1
Discretization errors (single-phase flow, heterogeneous domain, diagonal permeability tensor, structured grid).

$1/h$	$L^P_{\infty-integ}$ (MPFA-O)	$L^P_{2-integ}$ (MPFA-O)	$L^P_{\infty-integ}$ (TPFA)	$L^P_{2-integ}$ (TPFA)
8	3.30E+00	6.12E-01	3.30 E+00	6.12E-01
16	1.06 E+00	1.87E-01	1.06 E+00	1.87E-01
32	2.87E-01	5.05E-02	2.87E-01	5.05E-02
64	7.40E-02	1.31E-02	7.40E-02	1.31E-02
$O(L)$	1.83	1.85	1.83	1.85

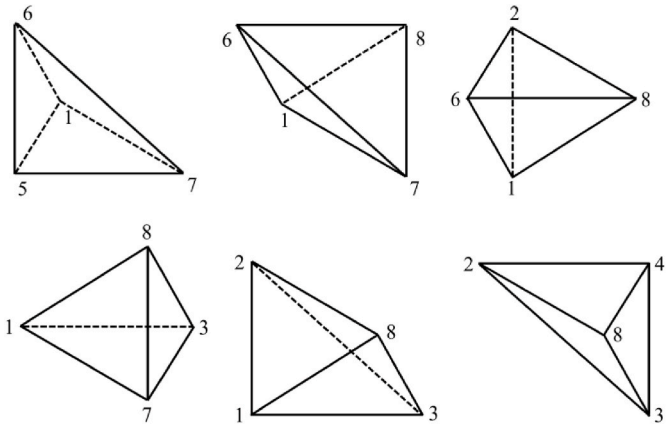

Fig. 9. Split a hexahedral grid into six tetrahedron grids.

been implemented in many commercial simulators. However, the complexity of the ensemble of the Jacobian brings hassles to software development when add/change governing physics (Cao, 2002). The automatic differentiation techniques (Voskov, 2012; Zaydullin et al., 2014; Garipov et al., 2016, 2018) are proven to provide robust solutions and help to keep the flexibility of a reservoir simulator. But the automatic differentiation usually introduces an overhead and limits the

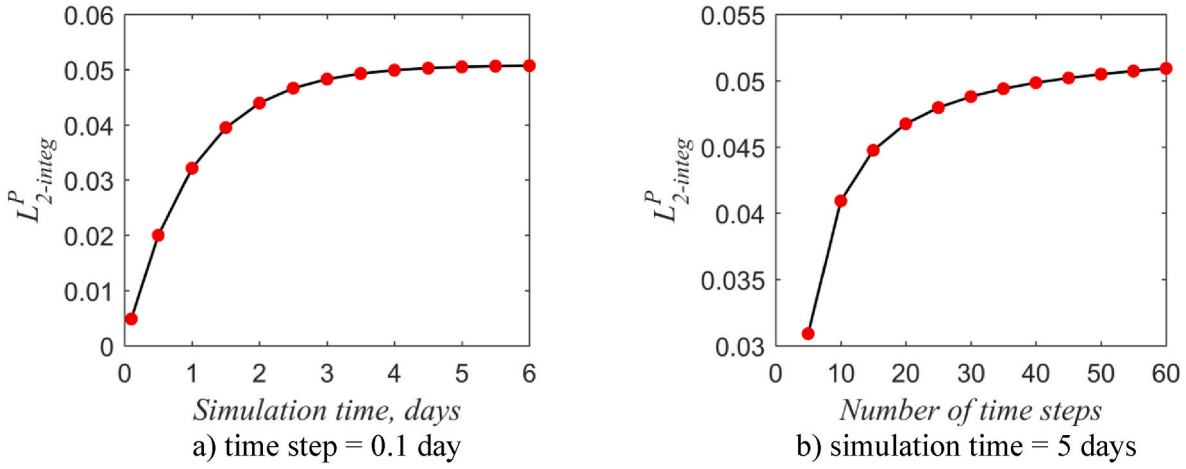

Fig. 7. The effect of simulation time and time step on errors.

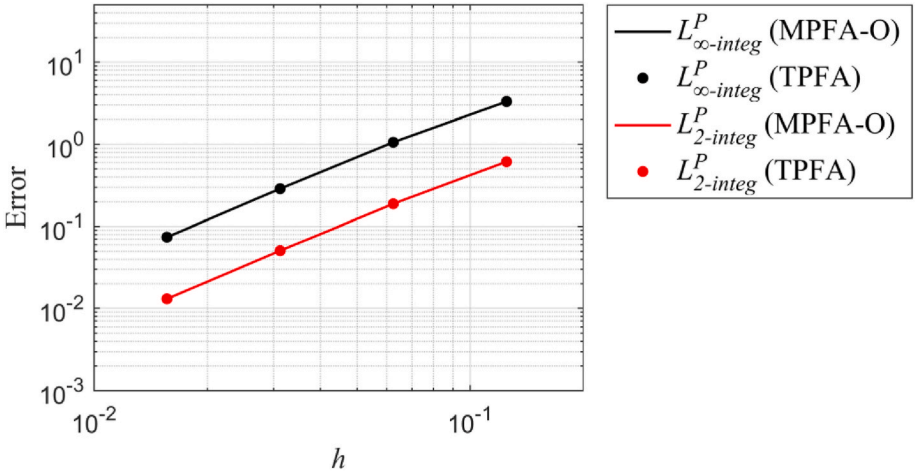

Fig. 8. Comparison of MPFA-O error to TPFA error, single-phase flow, heterogeneous domain, diagonal permeability tensor, structured grid.

Table 2
Discretization errors (single-phase flow, heterogeneous domain, diagonal permeability tensor, unstructured grid), h is the size of the hexahedral grid.

$1/h$	$L^P_{\infty-integ}$ (MPFA-O)	$L^P_{2-integ}$ (MPFA-O)	$L^P_{\infty-integ}$ (TPFA)	$L^P_{2-integ}$ (TPFA)
8	4.07 E+00	5.22E-01	2.71E+01	3.17 E+00
16	1.95 E+00	2.67E-01	2.74E+01	4.09 E+00
32	8.68E-01	1.13E-01	2.74E+01	4.59 E+00
64	2.60E-01	3.20E-02	2.77E+01	4.87 E+00
$O(L)$	1.32	1.34	−1.06E-02	−2.06E-01

efficiency of a reservoir simulator.

Recently, a novel linearization approach named Operator-based Linearization (OBL) has been proposed in (Voskov, 2017). In this approach, the operators, combining the fluid and rock properties, are introduced into the governing equations. Considering the fact that the operators account for the most complex and nonlinear part of the system, an additional discretization of the operators is introduced in the physical parameter space. Then, a piecewise linear representation of the physics simplifies the evaluation of the complex phase behavior as well as rock property. Also, a moderate coarsening of physics helps to reduce the nonlinearity of the system. The applications in various challenging problems prove the robustness and reliability of the OBL method (Khait and Voskov, 2016, 2017, 2018a, 2018b; Wang et al., 2020).

In this work, we first involve the advanced MPFA-O scheme and OBL approach within a parallel framework for general-purpose reservoir simulation. The MPFA-O method is applied on a general unstructured mesh for the purpose of handling complex geological models. The mass-based formulation employing OBL is involved in a fully implicit scheme to provide unconditionally stable solutions. Thanks to the implementation of OBL, the programming of the Jacobian assembly is simplified significantly. In order to enhance the modelling capabilities of high-fidelity/high-resolution geological models, we use massively parallel computations via Message Passing Interface (MPI) which can improve the simulation efficiency significantly. Finally, we present several benchmark cases under single-phase and two-phase flow and two challenging field-scale cases to demonstrate the accuracy, convergence, and computing performance of the new simulator.

2. Parallel framework for reservoir simulation

In this section, we describe the governing equations, discretization method, linearization method, and the implementation of the framework.

Table 3
Discretization errors (single-phase flow, heterogeneous domain, full permeability tensor, structured grid).

$1/h$	$L^P_{\infty-integ}$ (MPFA-O)	$L^P_{2-integ}$ (MPFA-O)	$L^P_{\infty-integ}$ (TPFA)	$L^P_{2-integ}$ (TPFA)
8	1.56E-03	5.00E-04	1.44E-01	4.68E-02
16	4.84E-04	1.63E-04	1.82E-01	6.17E-02
32	1.31E-04	4.57E-05	1.98E-01	6.98E-02
64	3.40E-05	1.21E-05	2.07E-01	7.40E-02
$O(L)$	1.84	1.79	−1.74E-01	−2.21E-01

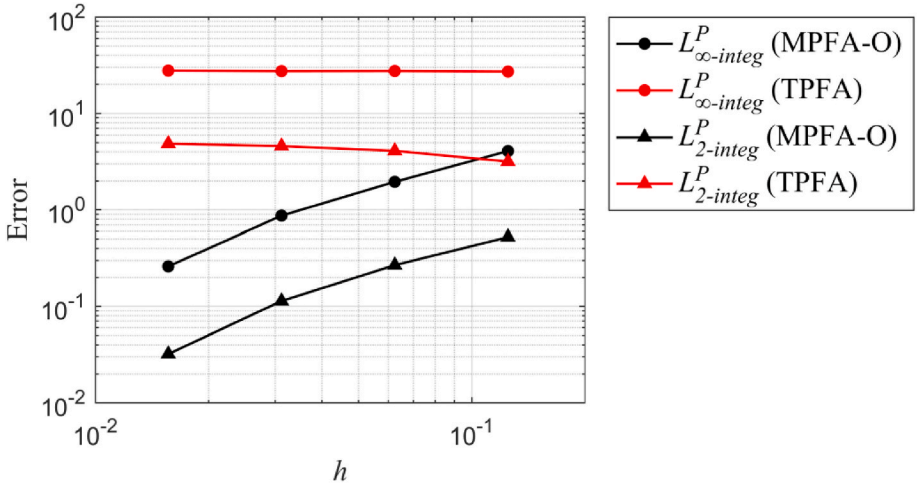

Fig. 10. Comparison of MPFA-O error to TPFA error, single-phase flow, heterogeneous domain, diagonal permeability tensor, unstructured grid.

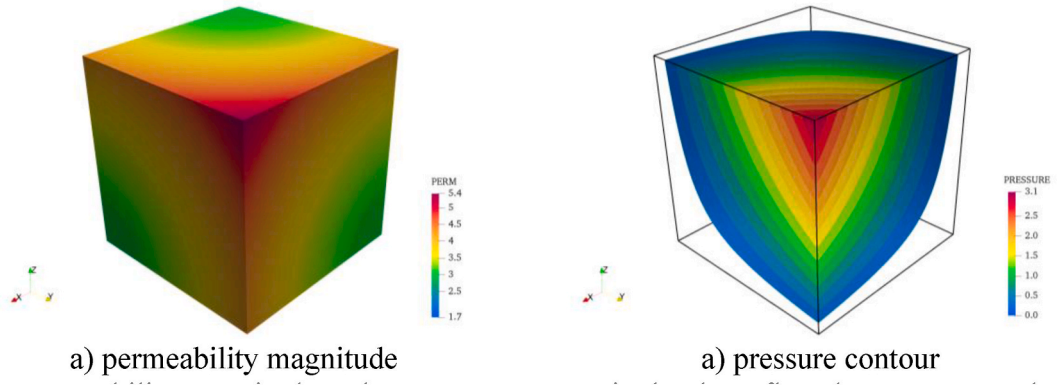

Fig. 11. Permeability magnitude and pressure contour, single-phase flow, heterogeneous domain, full permeability tensor.

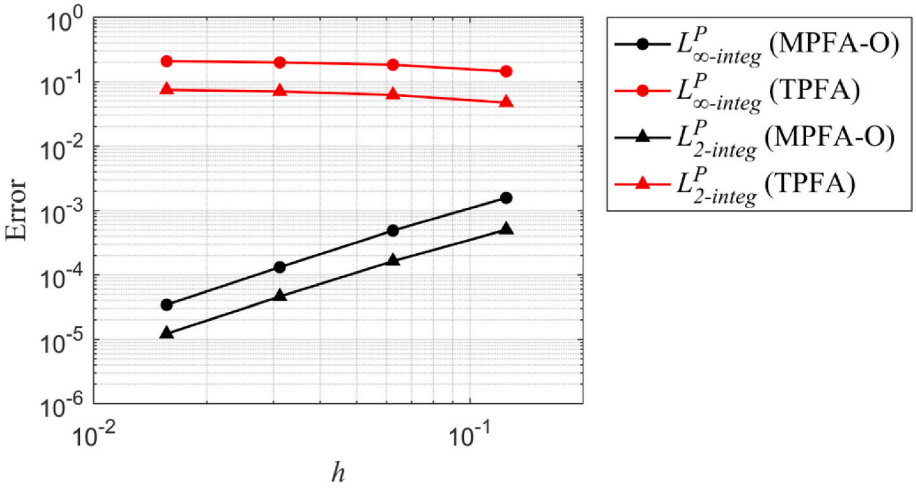

Fig. 12. Comparison of MPFA-O error to TPFA error, single-phase flow, heterogeneous domain, full permeability tensor, structured grid.

Table 4
Discretization errors (single-phase flow, heterogeneous domain, full permeability tensor, unstructured grid), h is the size of the hexahedral grid.

$1/h$	$L^P_{\infty-integ}$ (MPFA-O)	$L^P_{2-integ}$ (MPFA-O)	$L^P_{\infty-integ}$ (TPFA)	$L^P_{2-integ}$ (TPFA)
8	1.54E-03	3.27E-04	4.92E-02	1.36E-02
16	4.15E-04	9.56E-05	5.73E-02	1.93E-02
32	1.11E-04	2.60E-05	6.22E-02	2.34E-02
64	2.91E-05	6.79E-06	6.49E-02	2.59E-02
$O(L)$	1.91	1.86	−1.33E-01	−3.11E-01

2.1. Governing equations

A typical fluid model in petroleum, the black oil model (Li et al., 2004), is applied to describe the phase behavior underground. In this model, there are three components including a light hydrocarbon, a heavy hydrocarbon, and a water component. The two hydrocarbon components comprise the hydrocarbon system that has oil and gas phases while the water component only stays inside the aqueous phase. The light one, usually rich in methane, forms the gas phase. The heavy one mainly constitutes the liquid oil phase. To represent the mass transfer between gas and oil phases, a certain amount of the light hydrocarbon is allowed to be dissolved in the oil phase depending on pressure. The transport equations of the three components can be written as below.

$$\frac{\partial}{\partial t}\left[\varphi\left(\rho_g S_g + \frac{\rho_{gst}}{B_o} R_g S_o\right)\right] + \nabla\cdot\left(\lambda_g \rho_g \mathrm{K}\nabla P + \lambda_o \frac{\rho_{gst}}{B_o} R_g \mathrm{K}\nabla P\right) + q_g = 0, \quad (1)$$

$$\frac{\partial}{\partial t}(\varphi\rho_o S_o) + \nabla\cdot(\lambda_o \rho_o \mathrm{K}\nabla P) + q_o = 0, \quad (2)$$

$$\frac{\partial}{\partial t}(\varphi\rho_w S_w) + \nabla\cdot(\lambda_w \rho_w \mathrm{K}\nabla P) + q_w = 0. \quad (3)$$

where φ is the reservoir porosity; t is the time; subscripts g, o, and w represent gas, oil, and water; subscript st represents the standard condition; ρ is the phase density; B is the formation volume factor; S is the saturation; λ is the phase mobility which is defined as k_{ro}/μ_o in oil phase; k_{ro} is the relative permeability of oil phase; μ is the viscosity; P is the pressure; $\mathbf{K}$ is the effective permeability tensor; q is the phase rate per unit volume; R_g is the gas solubility that represents the mass transfer between gas and oil phases.

Table 5
parameters for simulation.

	K [mD]	Φ	μ_o	μ_w	n_o	n_w
value	1	0.3	2	1	2	2

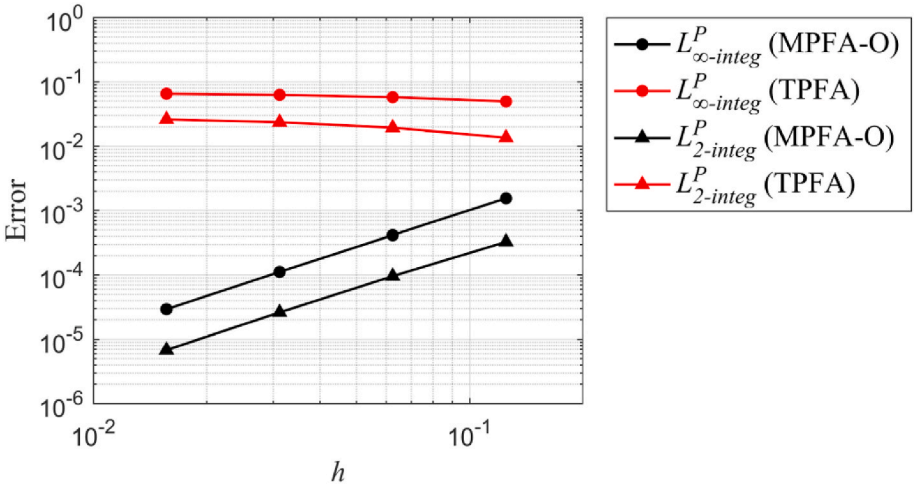

Fig. 13. Comparison of MPFA-O error to TPFA error, single-phase flow, heterogeneous domain, full permeability tensor, unstructured grid.

Equation (4) is applied to close the system.

$$S_g + S_o + S_w = 1. \tag{4}$$

2.2. Discretization employing multipoint flux approximation method

Taking full use of complex geological models is always challenging for reservoir simulation. First, unstructured gridding is sometimes required to characterize the important features explicitly; second, a coarsening of high-resolution heterogeneous geological model could introduce full tensor permeability. In this work, to tackle these two challenges, we apply the MPFA-O method for discretization assisted with the functions related to geometry calculation in INMOST (Terekhov and Vassilevski, 2019).

Take the mesh in Fig. 1 for example, there are six control volumes in black bold lines and two intersection volumes in red lines. Points x_1, x_2, x_3, x_4, x_5, and x_6 are the centers of cell 1, cell 2, cell 3, cell 4, cell 5, and cell 6; points $\overline{x}_1$, $\overline{x}_2$, $\overline{x}_3$, $\overline{x}_4$, $\overline{x}_5$, $\overline{x}_6$, and $\overline{x}_7$ are the midpoints of edges where the subscripts indicate serial number. The fluxes through half-edges including $\overline{x}_1x_7$, $\overline{x}_3x_7$, $x_7\overline{x}_2$, and $x_7\overline{x}_4$ are computed through intersection volume $x_1x_2x_4x_3$, and the fluxes through half-edges including $\overline{x}_2x_8$, $\overline{x}_6x_8$, $x_8\overline{x}_5$, and $x_8\overline{x}_7$ are computed through intersection volume $x_3x_4x_6x_5$. Next, we describe the computation in detail with the lower intersection volume.

As shown in Fig. 2, $\mathbf{v}$ is the normal vector on the half-edges of intersection volumes; take $\mathrm{v}_1^{(1)}$ as an example, it is a normal on the connection line between x_1 and $\overline{x}_3$, the superscript denotes the index of cell 1; $\mathbf{n}_1$, $\mathbf{n}_2$, $\mathbf{n}_3$, and $\mathbf{n}_4$ are the normal vectors on the half-edges of control volumes. Here, we approximately take the pressure gradient in triangular $x_1\overline{x}_1\overline{x}_3$ as in sub-region $x_1\overline{x}_1x_7\overline{x}_3$. Then, the pressure in this region can be computed as described below:

$$P = a_1\overline{P}_1 + a_2\overline{P}_3 + (1 - a_1 - a_2)P_1, \tag{5}$$

where $\overline{P}_1$ and $\overline{P}_3$ are the pressure on points $\overline{x}_1$ and $\overline{x}_3$; P_1 is the pressure on point x_1; a_1 and a_2 are linear functions. The gradient of a_1 in the direction of $\mathrm{v}_1^{(1)}$ and the gradient of a_2 in the direction of $\mathrm{v}_2^{(1)}$ can be written as:

$$\mathrm{grad}a_1 = \frac{1}{2F_1}\mathrm{v}_1^{(1)}, \mathrm{grad}a_2 = \frac{1}{2F_1}\mathrm{v}_2^{(1)}, \tag{6}$$

where F_1 is the area of the triangle $x_1\overline{x}_1\overline{x}_3$. Thus, the pressure gradient may be written in the form:

$$\mathrm{grad}P = \frac{1}{2F_1}\left[\mathrm{v}_1^{(1)}(\overline{P}_1 - P_1) + \mathrm{v}_2^{(1)}(\overline{P}_3 - P_1)\right]. \tag{7}$$

Based on the pressure gradient, we next compute the fluxes $f_1^{(1)}$ and $f_3^{(1)}$ through half-edges $\overline{x}_1x_7$ and $\overline{x}_3x_7$. The superscript and subscript of f indicate the indexes of cell and half-edge respectively.

$$\begin{bmatrix} f_1^{(1)} \\ f_3^{(1)} \end{bmatrix} = -\begin{bmatrix} \Gamma_1\mathbf{n}_1^T \\ \Gamma_3\mathbf{n}_3^T \end{bmatrix}\mathrm{K}_1\mathrm{grad}P = -\frac{1}{2F_1}\begin{bmatrix} \Gamma_1\mathbf{n}_1^T \\ \Gamma_3\mathbf{n}_3^T \end{bmatrix}\mathrm{K}_1\begin{bmatrix} \mathrm{v}_1^{(1)} & \mathrm{v}_2^{(1)} \end{bmatrix}\begin{bmatrix} \overline{P}_1 - P_1 \\ \overline{P}_3 - P_1 \end{bmatrix}, \tag{8}$$

where $\mathbf{K}_1$ is the permeability of cell 1 in full tensor format; Γ is the length of half-edge.

By defining G_1

$$G_1 = \frac{1}{2F_1}\begin{bmatrix} \Gamma_1\mathbf{n}_1^T \\ \Gamma_3\mathbf{n}_3^T \end{bmatrix}\mathrm{K}_1\begin{bmatrix} \mathrm{v}_1^{(1)} & \mathrm{v}_2^{(1)} \end{bmatrix} = \frac{1}{2F_1}\begin{bmatrix} \Gamma_1\mathbf{n}_1^T\mathrm{K}_1\mathrm{v}_1^{(1)} & \Gamma_1\mathbf{n}_1^T\mathrm{K}_1\mathrm{v}_2^{(1)} \\ \Gamma_3\mathbf{n}_3^T\mathrm{K}_1\mathrm{v}_1^{(1)} & \Gamma_3\mathbf{n}_3^T\mathrm{K}_1\mathrm{v}_2^{(1)} \end{bmatrix}, \tag{9}$$

Equation (8) can be written as

$$\begin{bmatrix} f_1^{(1)} \\ f_3^{(1)} \end{bmatrix} = -G_1\begin{bmatrix} \overline{P}_1 - P_1 \\ \overline{P}_3 - P_1 \end{bmatrix}. \tag{10}$$

Similarly, we obtain matrixes G_2, G_3, and G_4 in the sub-regions $\overline{x}_1x_2\overline{x}_4x_7$, $\overline{x}_3x_7\overline{x}_2x_3$, and $x_7\overline{x}_4x_4\overline{x}_2$. Then, the fluxes through half-edges in the four sub-regions can be written as:

$$\begin{aligned} &\begin{bmatrix} f_1^{(1)} \\ f_3^{(1)} \end{bmatrix} = -G_1\begin{bmatrix} \overline{P}_1 - P_1 \\ \overline{P}_3 - P_1 \end{bmatrix}, \begin{bmatrix} f_1^{(2)} \\ f_4^{(2)} \end{bmatrix} = -G_2\begin{bmatrix} P_2 - \overline{P}_1 \\ \overline{P}_4 - P_2 \end{bmatrix} \\ &\begin{bmatrix} f_2^{(3)} \\ f_3^{(3)} \end{bmatrix} = -G_3\begin{bmatrix} \overline{P}_2 - P_3 \\ P_3 - \overline{P}_3 \end{bmatrix}, \begin{bmatrix} f_2^{(4)} \\ f_4^{(4)} \end{bmatrix} = -G_4\begin{bmatrix} P_4 - \overline{P}_2 \\ P_4 - \overline{P}_4 \end{bmatrix}. \end{aligned} \tag{11}$$

Assuming that the flux on the interface of two neighboring cells is continuous, equation (11) can be rewritten as:

$$\begin{aligned} f_1 &= -g_{1,1}^{(1)}(\overline{P}_1 - P_1) - g_{1,2}^{(1)}(\overline{P}_3 - P_1) = g_{1,1}^{(2)}(\overline{P}_1 - P_2) - g_{1,2}^{(2)}(\overline{P}_4 - P_2) \\ f_2 &= g_{1,1}^{(4)}(\overline{P}_2 - P_4) + g_{1,2}^{(4)}(\overline{P}_4 - P_4) = -g_{1,1}^{(3)}(\overline{P}_2 - P_3) + g_{1,2}^{(3)}(\overline{P}_3 - P_3) \\ f_3 &= -g_{2,1}^{(3)}(\overline{P}_2 - P_3) + g_{2,2}^{(3)}(\overline{P}_3 - P_3) = -g_{2,1}^{(1)}(\overline{P}_1 - P_1) - g_{2,2}^{(1)}(\overline{P}_3 - P_1) \\ f_4 &= g_{2,1}^{(2)}(\overline{P}_1 - P_2) - g_{2,2}^{(2)}(\overline{P}_4 - P_2) = g_{2,1}^{(4)}(\overline{P}_2 - P_4) + g_{2,2}^{(4)}(\overline{P}_4 - P_4) \end{aligned} \tag{12}$$

where g is the submatrix of G and its superscript is the index of the cell.

By defining $\mathrm{f} = [f_1, f_2, f_3, f_4]^{\mathrm{T}}$, $\mathrm{P} = [P_1, P_2, P_3, P_4]^{\mathrm{T}}$, and $\overline{\mathrm{P}} = [\overline{P}_1, \overline{P}_2, \overline{P}_3, \overline{P}_4]^{\mathrm{T}}$, we can derive two equations based on Equation (12):

$$\mathrm{f} = \mathrm{C}\overline{\mathrm{P}} + \mathrm{F}\mathrm{P}, \tag{13}$$

and

$$\mathrm{A}\overline{\mathrm{P}} = \mathrm{B}\mathrm{P}. \tag{14}$$

where

$$\mathrm{A} = \begin{bmatrix} -g_{1,1}^{(1)} - g_{1,1}^{(2)} & 0 & -g_{1,2}^{(1)} & g_{1,2}^{(2)} \\ 0 & g_{1,1}^{(4)} + g_{1,1}^{(3)} & -g_{1,2}^{(3)} & g_{1,2}^{(4)} \\ g_{2,1}^{(1)} & -g_{2,1}^{(3)} & g_{2,2}^{(3)} + g_{2,2}^{(1)} & 0 \\ g_{2,1}^{(2)} & -g_{2,1}^{(4)} & 0 & -g_{2,2}^{(2)} - g_{2,2}^{(4)} \end{bmatrix}, \tag{15}$$

$$\mathrm{B} = \begin{bmatrix} -g_{1,1}^{(1)} - g_{1,2}^{(1)} & -g_{1,1}^{(2)} + g_{1,2}^{(2)} & 0 & 0 \\ 0 & 0 & g_{1,1}^{(3)} - g_{1,2}^{(3)} & g_{1,1}^{(4)} + g_{1,2}^{(4)} \\ g_{2,1}^{(1)} + g_{2,2}^{(1)} & 0 & -g_{2,1}^{(3)} + g_{2,2}^{(3)} & 0 \\ 0 & g_{2,1}^{(2)} - g_{2,2}^{(2)} & 0 & -g_{2,1}^{(4)} - g_{2,2}^{(4)} \end{bmatrix}, \tag{16}$$

$$\mathrm{C} = \begin{bmatrix} -g_{1,1}^{(1)} & 0 & -g_{1,2}^{(1)} & 0 \\ 0 & g_{1,1}^{(4)} & 0 & g_{1,2}^{(4)} \\ 0 & -g_{2,1}^{(3)} & g_{2,2}^{(3)} & 0 \\ g_{2,1}^{(2)} & 0 & 0 & -g_{2,2}^{(2)} \end{bmatrix}, \tag{17}$$

$$\mathrm{F} = \begin{bmatrix} g_{1,1}^{(1)} + g_{1,2}^{(1)} & 0 & 0 & 0 \\ 0 & 0 & 0 & -g_{1,1}^{(4)} - g_{1,2}^{(4)} \\ 0 & 0 & g_{2,1}^{(3)} - g_{2,2}^{(3)} & 0 \\ 0 & -g_{2,1}^{(2)} + g_{2,2}^{(2)} & 0 & 0 \end{bmatrix}. \tag{18}$$

By combining Equations (13) and (14), we can obtain:

$$\mathrm{f} = \mathrm{T}\mathrm{P}, \mathrm{T} = \mathrm{C}\mathrm{A}^{-1}\mathrm{B} + \mathrm{F}. \tag{19}$$

Table 6
Simulation results using different OBL resolutions.

OBL resolution	Absolute error of Sw (T = 1000 days)	Total nonlinear newton iterations	Nonlinear newton iterations per time steps		$CFL_{\infty max}$
2	3.05E-01	20,024	2.00E+00	7.37E-01	1.67E+00
4	5.17E-02	20,669	2.07E+00	5.68E-01	1.22E+00
8	1.83E-02	22,320	2.23E+00	6.95E-01	1.09E+00
16	7.76E-03	30,027	3.00E+00	7.80E-01	1.04E+00
32	2.74E-03	31,081	3.11E+00	8.48E-01	1.02E+00
64	7.83E-04	33,767	3.37E+00	8.99E-01	1.19E+00
128	1.75E-04	34,620	3.46E+00	9.56E-01	1.43E+00
256	2.77E-05	35,491	3.55E+00	9.77E-01	1.77E+00
Conventional	0	35,226	3.52E+00	1.36E+00	2.06E+00

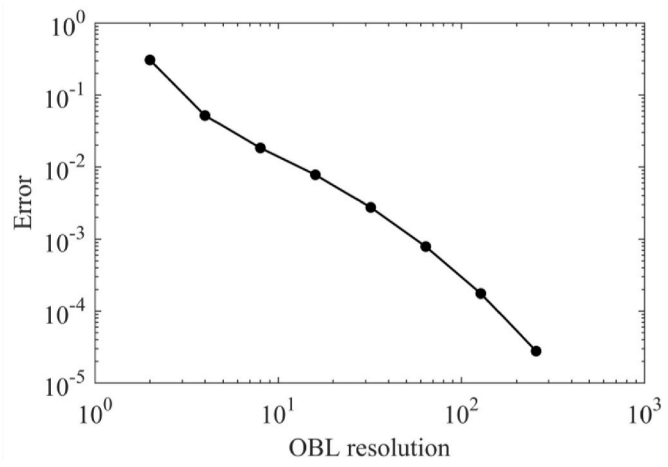

Fig. 14. The effect of OBL resolution on the absolute error of water saturation, $T = 1000$ days.

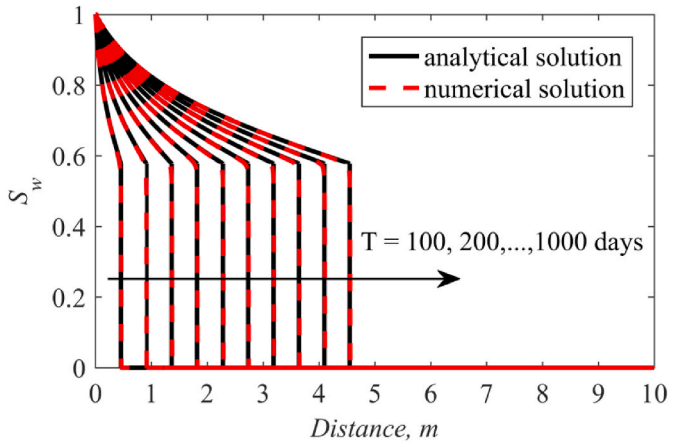

Fig. 15. Comparison of analytical solutions to numerical solutions at different simulation time, OBL resolution is 64.

As knowing the fluxes through full-edges could benefit the implementation of MPFA-O a lot, we derive a new formulation based on Equation (19):

$$f_{integ} = \mathrm{T}_{integ}\mathrm{P}_{integ}. \tag{20}$$

Taking the connection between cell 3 and cell 4 in Fig. 1 as an example, Equation (20) can be instantiated as:

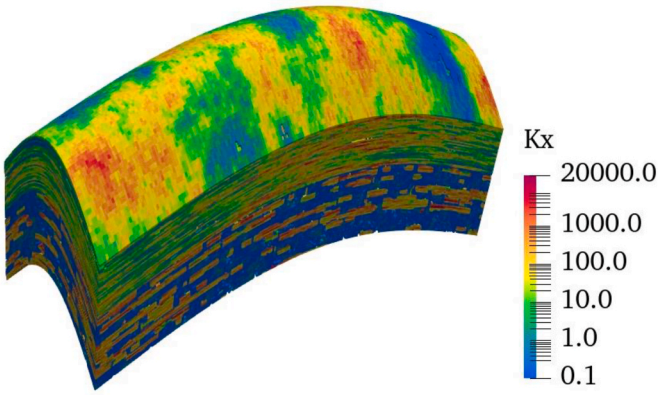

Fig. 16. Permeability distribution of the bent SPE10 model.

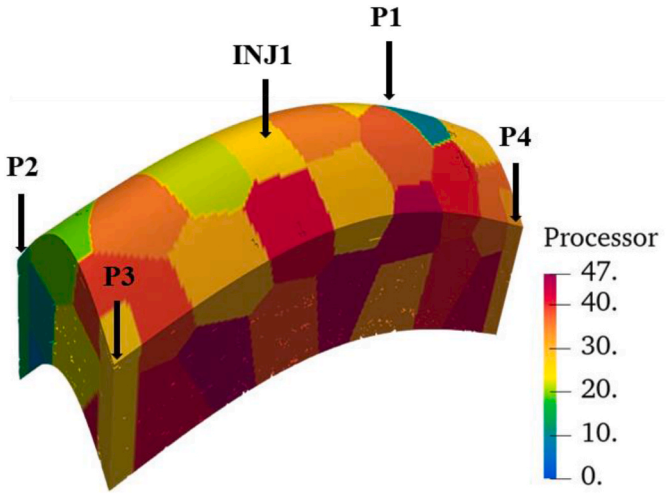

Fig. 17. Domain decomposition of the bent SPE10 model, 48 subdomains.

$$f_{c3-c4} = \begin{bmatrix} T_{1integ} \\ T_{2integ} \\ T_{3integ} \\ T_{4integ} \\ T_{5integ} \\ T_{6integ} \end{bmatrix}^T \begin{bmatrix} P_1 \\ P_2 \\ P_3 \\ P_4 \\ P_5 \\ P_6 \end{bmatrix}. \tag{21}$$

In this way, we can construct the transmissibility vector and its corresponding grid information in the connection-based approach (Cao, 2002; Terekhov et al., 2017).

Then, the governing Equations (1)–(3) can be transformed as follows when applying Equation (20) to discretize in space and applying backward Euler approximation to discretize in time.

$$\begin{aligned} &\left[V\varphi\left(\rho_g S_g + \frac{\rho_{gst}}{B_o}R_g S_o\right)\right]^{n+1} - \left[V\varphi\left(\rho_g S_g + \frac{\rho_{gst}}{B_o}R_g S_o\right)\right]^{n} \\ &-\Delta t\sum_l\left[\left(\lambda_g^l\rho_g^l + \lambda_o^l\frac{\rho_{gst}}{B_o^l}R_g^l\right)\mathrm{T}_{integ}^l\mathrm{P}_{integ}^l\right] + \Delta t V q_g = 0, \end{aligned} \tag{22}$$

$$(V\varphi\rho_o S_o)^{n+1} - (V\varphi\rho_o S_o)^{n} - \Delta t\sum_l\left(\lambda_o^l\rho_o^l\mathrm{T}_{integ}^l\mathrm{P}_{integ}^l\right) + \Delta t V q_o = 0, \tag{23}$$

$$(V\varphi\rho_w S_w)^{n+1} - (V\varphi\rho_w S_w)^{n} - \Delta t\sum_l\left(\lambda_w^l\rho_w^l\mathrm{T}_{integ}^l\mathrm{P}_{integ}^l\right) + \Delta t V q_w = 0. \tag{24}$$

Here, V is the volume of a grid block; l denotes the interfaces between a grid block and its neighboring grid blocks; $\lambda_j^l = (k_{rj}/\mu_j)^l$ is the mobility of

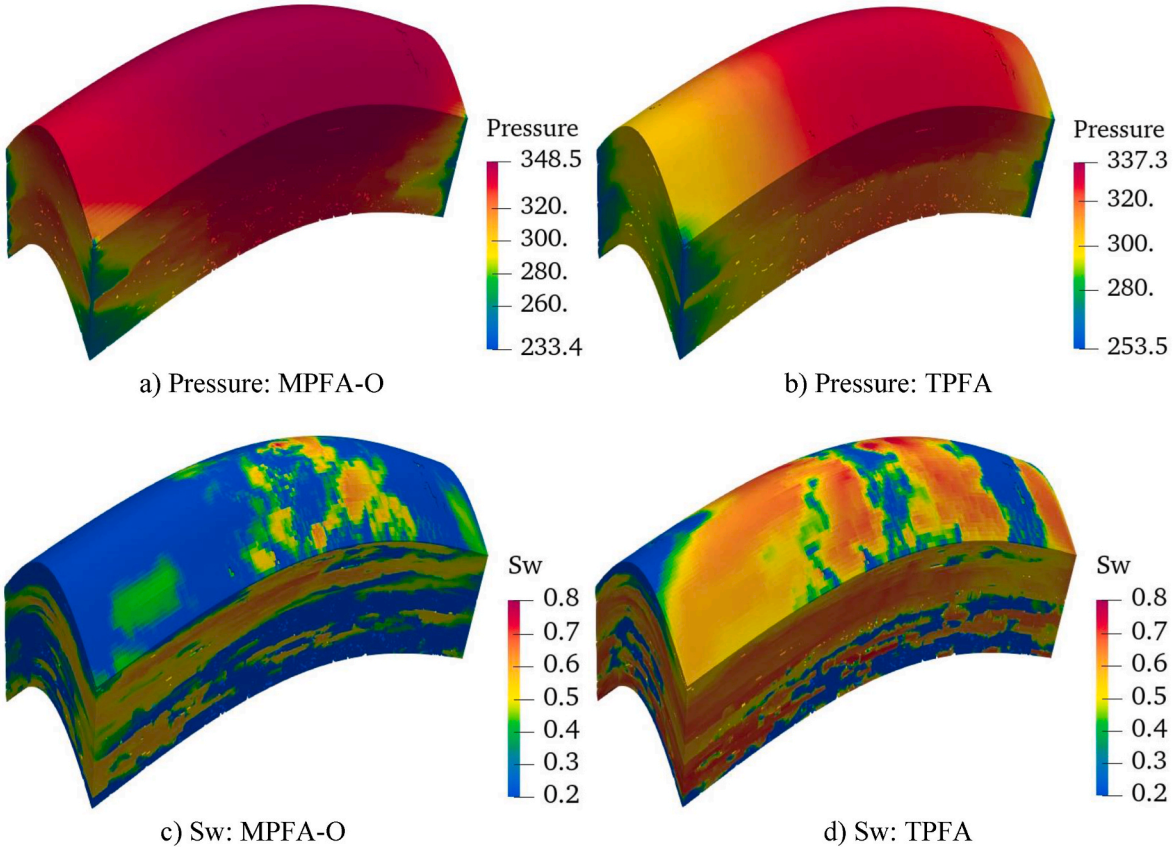

Fig. 18. Case 1 the pressure and water saturation distributions.

phase j over the interface l by the classic upstream weighting; n+1 is the current time step; n is the previous time step. It is good to mention that the arithmetic mean of mobilities (Souza et al., 2018) is also a good strategy to approximate the mobility.

2.3. Operator-based representation of governing equations

In this section, to simplify the representation of governing equations, we re-write Eqs. (22)–(24) in a general form (Voskov, 2017).

$$V(\boldsymbol{\xi})\varphi_0(\boldsymbol{\xi})[\alpha_c(\boldsymbol{\omega})-\alpha_c(\boldsymbol{\omega}_n)]-\sum_l \Delta t\mathbf{T}^l_{integ}\mathbf{P}\beta^l_c(\boldsymbol{\omega})+\Delta tVq_c=0, c=1,2,3, \tag{25}$$

where ξ is the spatial coordinate, ω is the physical state. The operators are defined as:

$$\alpha_1(\omega)=\left[1+c_r\left(P-P_{ref}\right)\right]\left(\rho_g S_g+\frac{\rho_{gst}}{B_o}R_g S_o\right), \tag{26}$$

$$\alpha_2(\omega)=\left[1+c_r\left(P-P_{ref}\right)\right]\rho_o S_o, \tag{27}$$

$$\alpha_3(\omega)=\left[1+c_r\left(P-P_{ref}\right)\right]\rho_w S_w, \tag{28}$$

$$\beta_1(\omega)=\lambda^l_g\rho^l_g+\lambda^l_o\frac{\rho_{gst}}{B^l_o}R^l_g, \tag{29}$$

$$\beta_2(\omega)=\lambda^l_o\rho^l_o, \tag{30}$$

$$\beta_3(\omega)=\lambda^l_w\rho^l_w, \tag{31}$$

Here, P_{ref} is the reference pressure for the porosity φ_0; c_r is the rock compressibility factor. The operators α_c and β_c are only dependent on the phase and rock properties and independent of spatially distributed properties.

The operator-based representation of governing equations provides a way to unify the three governing equations. What is more, it could also unify the governing equations of different models such as single-phase, two-phase dead oil, three-phase black oil, and compositional models. A programming based on this kind of representation helps to keep the flexibility and extensibility of the simulator. Besides, the most severe nonlinearity and complexity related to phase behavior and property calculation can be reduced to evaluation of operators.

2.4. Fully implicit scheme using the OBL

Induced by the complex geological model and phase behavior underground, the flow system in petroleum is quite nonlinear. Thus, we apply the unconditionally stable fully implicit method in this framework to guarantee robust solutions. It can be written as below with the application of the Newton-Raphson method.

$$\mathrm{x}^{k+1}_{n+1}=\mathrm{x}^k_{n+1}-\frac{\mathrm{r}\left(\mathrm{x}^k_{n+1}\right)}{\mathrm{J}\left(\mathrm{x}^k_{n+1}\right)}, \tag{32}$$

where $\mathbf{x}$ is the vector of unknowns; the subscript n+1 represents the current time step; the superscript k and k+1 represent previous nonlinear iteration and current nonlinear iteration respectively; $\mathrm{r}(\mathrm{x}^k_{n+1})$ and $\mathrm{J}(\mathrm{x}^k_{n+1})$ are the residual vector and Jacobian matrix evaluated using the estimated unknowns at k nonlinear iteration.

In the operator-based linearization (OBL) approach (Voskov, 2017), the molar formulation is applied for solving the system of Equation (25). For the black oil model, the nonlinear unknowns are comprised of

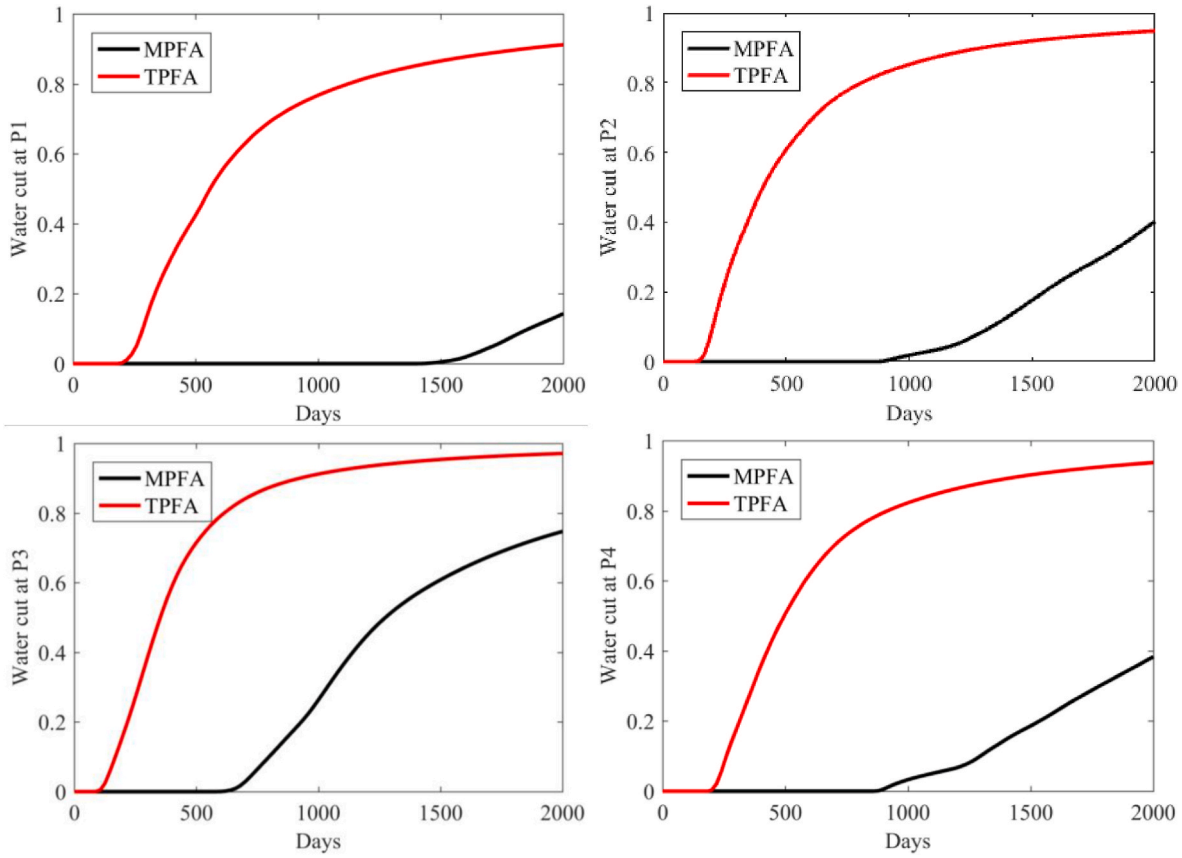

Fig. 19. Case 1 water cut of production wells.

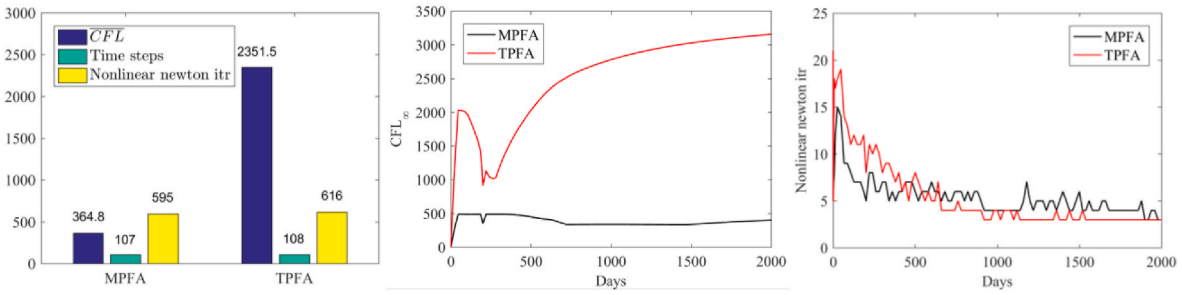

Fig. 20. Case 1 computational results of MPFA-O and TPFA schemes.

Table 7
Well locations.

Well name	INJ	P1	P2	P3	P4
X	202	122	82	362	290
Y	222	82	402	82	342

pressure, mass overall composition of gas component z_g, mass overall composition of oil component z_o. It is worth mentioning that the unknowns are exactly the physical state which can be used to compute the properties in operators α_c and β_c.

Benefit from that, the operators can be represented in an explicit and effective manner when we discretize the parameter space of the unknowns using a uniform grid and estimate the values of the operators on the vertices. With regard to the points not coinciding with the vertices, the values of their operators can be evaluated by multi-linear interpolation. The interpolation coefficients will yield partial derivatives of operators with respect to nonlinear unknowns. Here, we take a black oil system to illustrate the theory. In this example, a three-dimensional space, with pressure, z_g, and z_o on each axis, is discretized uniformly. By setting the number of points (resolution) on each axis equal to 32, we compute all operators in the vertices. Here, for an illustrative visualization, we only show four cross-sections in the direction of pressure in Fig. 3. The smoothly distributed operators, represented by the degree of color, demonstrate the feasibility of the OBL.

In this work, following an adaptive way proposed in (Khait and Voskov, 2017), the operators on each node are only computed single time and stored when a physical state falls inside its supporting hypercubes during a simulation run. Compared with the traditional

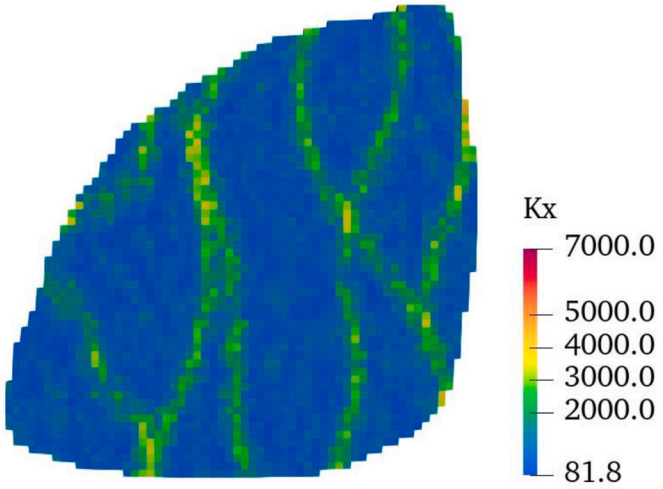

Fig. 21. Permeability distribution of egg model.

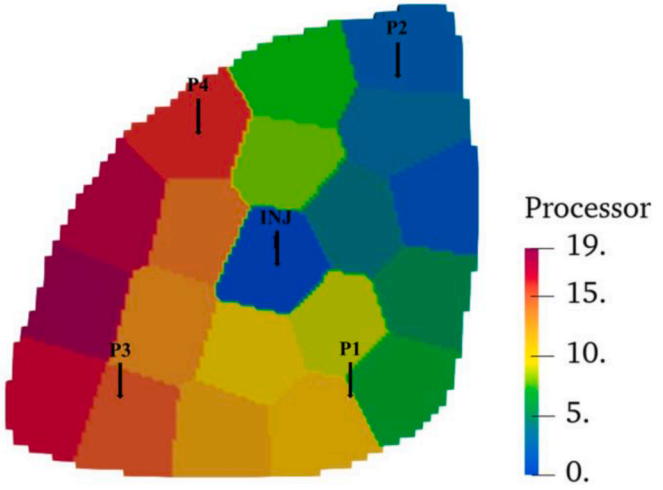

Fig. 22. Domain decomposition of egg model, 20 subdomains.

approaches such as numerical differentiation, hand-differentiation or automatic differentiation techniques, the OBL approach reduces the time spent on property computations (e.g. complex phase behavior) quite a lot.

2.5. Implementation of MPFA-O and OBL within a parallel framework

To guarantee efficient solutions for reservoir simulation, we implement state-of-the-art MPFA-O and OBL methods within a parallel modelling framework (Li et al., 2020; Li and Abushaikha, 2020; Li and Abushaikha, 2022). In this framework, we apply the MPI standard for parallel communication because of its feasibilities in distributed and shared memory systems. The point-to-point communication benefits the construction of distributed mesh and the update of nonlinear unknowns in ghost cells greatly. Fig. 4 shows a flowchart for the implementation work which is described in detail as follows..

(1) Input. We read the simulation parameters and load the mesh with geological information.
(2) Domain decomposition (DDM). We divide the global reservoir domain into sub-domains according to the number of processors required for simulation. In this study, the K-MEANS and Reverse Cuthill-McKee algorithm (RCM) methods are applied for DDM. Moreover, the other algorithms from the Zoltan library can also be involved in this framework. Taking a geological model with 8 × 8 structured grids as an example, four sub-domains, shown in Fig. 5a, can be partitioned employing the Recursive Coordinate Bisection (RCB) method.
(3) Construction of shared and ghost cells. The flux through a face lying on the interface of two neighboring sub-domains is constrained by the grid pressures from two or more sub-domains in the MPFA-O scheme. Thus, the communication of mesh information and grid nonlinear unknonwns between neighboring sub-domains is required. Aim to solve that, we determine shared cells in blue in Fig. 5b of which the unknowns and properties will be sent to neighboring sub-domains. Moreover, we construct ghost cells in red in Fig. 5c to receive the information. Besides, we show the mesh of TPFA scheme in Fig. 5d as a comparison. We can find that the work related to the construction of shared and ghost cells for MPFA-O is more complicated that for TPFA, especially when we use unstructured mesh.
(4) Discretization. We construct the matrix $\mathbf{T}_{integ}$ for flux computation on each face employing the MPFA-O scheme described above.
(5) Coupling wells. We find the reservoir blocks penetrated by the wells and calculate the well index.
(6) Solution process. In each time step, we converge the solution below the pre-defined tolerance using nonlinear newton-based solver. For the system at each nonlinear iteration, we linearize it with OBL approach. However, the linear system could be nonsymmetric because of the application of MPFA-O scheme and source/sink term. In this study, we apply the biconjugate gradient stabilized method (BiCGSTAB) (Van der Vorst, 1992) to solve the linear system. Besides, the Portable Extensible Toolkit for Scientific computation (PETSc) (Abhyankar Adams et al., 2014) linear solvers can also be employed to guatantee the solving capabilities for general-purpose reservoir simulation.
(7) Output. We output the computational results for further analysis and utilization.

3. Numerical benchmark

In this section, we present several numerical tests to demonstrate the accuracy and convergence of the framework's solutions. First, we investigate the convergence of numerical solutions to an analytical solution for single-phase flow in a heterogeneous domain; second, we extend the first case to a full tensor permeability case; third, to validate the feasibility of OBL method in multi-phase flow problems, we test the convergence of numerical solutions to a Buckley-Leverett analytical solution with respect to OBL resolution.

To conduct the accuracy and convergence study, we apply the following norms to quantify the differences between the numerical solution and analytical solution.

$$L^P_{\infty-integ} = \int_{t=0}^{T} L^P_\infty dt, L^P_\infty = \max_{1\le i\le N} |P_{a-i} - P_{n-i}|, \tag{33}$$

$$L^P_{2-integ} = \int_{t=0}^{T} L^P_2 dt, L^P_2 = \sqrt{\sum_{i=1}^{N} V_i (P_{a-i} - P_{n-i})^2}. \tag{34}$$

Where V_i is the volume of the ith grid block; $P_{a\text{-}i}$ is the analytical pressure solution of the ith block; $P_{n\text{-}i}$ is the numerical pressure solution of the ith block; N is the number of blocks. Note that L^P_∞ and L^P_2 are used for quantification at a certain time step or steady-state while $L^P_{\infty-integ}$ and

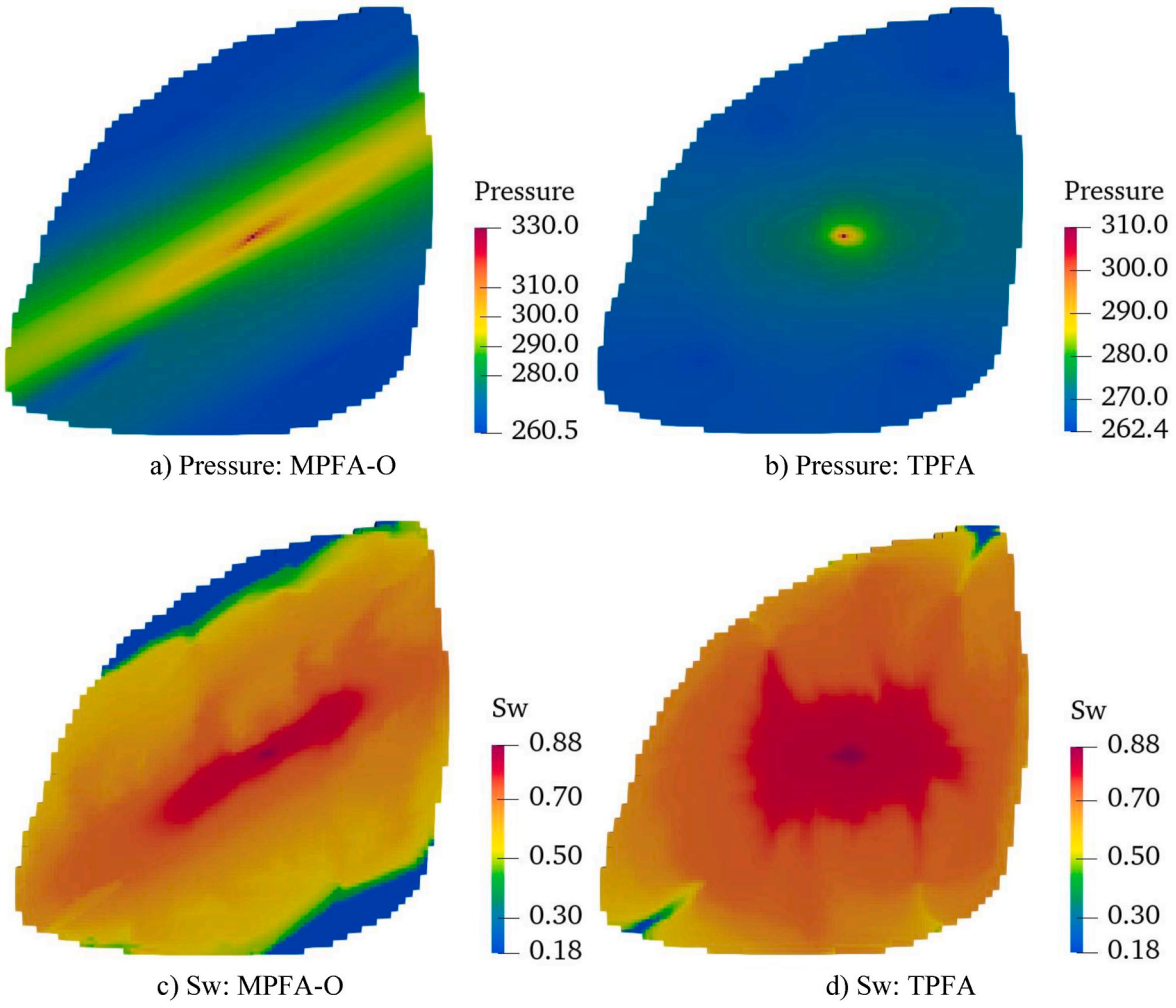

Fig. 23. Case 2 the pressure and water saturation distributions.

$L^P_{2-integ}$ are applied for transient state cases.

3.1. Single-phase flow in a heterogeneous domain

In this test, we consider a single-phase transient flow problem in a cubic heterogeneous domain with diagonal permeability tensor described by Equation (35).

$$\mathrm{K} = \begin{bmatrix} K_x & 0 & 0 \\ 0 & K_y & 0 \\ 0 & 0 & K_z \end{bmatrix}, \begin{cases} K_x = 1, K_y = 10, K_z = 0.01; & \Omega_1 = (0 \le y \le 0.5, 0 \le z \le 0.5) \\ K_x = 1, K_y = 0.1, K_z = 100; & \Omega_2 = (0.5 < y \le 1, 0 \le z \le 0.5) \\ K_x = 1, K_y = 0.01, K_z = 10; & \Omega_3 = (0.5 < y \le 1, 0.5 < z \le 1) \\ K_x = 1, K_y = 100, K_z = 0.1; & \Omega_4 = (0 \le y \le 0.5, 0.5 < z \le 1) \end{cases}. \tag{35}$$

The flow equation can be written as:

$$\nabla \cdot (\mathrm{K} \nabla P) = f, \tag{36}$$

where f is a force term constrained by an analytical solution:

$$P_a = a_i \sin(2\pi x)\sin(2\pi y)\sin(2\pi z)e^{-t}. \tag{37}$$

Here, t is the time which makes the force term time-dependent. Taking the analytical solution as a reference, we study the performance of the framework using structured and unstructured grids.

3.1.1. Structured grid

Here, we apply a hexahedral grid, shown in Fig. 6, with different grid resolutions shown in Table 1 to investigate the convergence of numerical solutions. To provide reliable solutions for analysis, we first determine optimal simulation time and time step with the third resolution ($1/h = 32$). In Fig. 7a, we apply a fixed time step (0.1 days) to study the effect of simulation time on error $L^P_{2-integ}$. We also employ a similar approach in Fig. 7b to investigate the sensitivity to time step with a fixed simulation time (5 days). Based on that, we determine the optimal simulation time and time step as 5 days and 0.1 days respectively. Any prolongation of simulation time or chop of time step will barely change the errors.

By comparing numerical solutions with the analytical solution at different scales, we obtain the $L^P_{\infty-integ}$ and $L^P_{2-integ}$ of MPFA-O and TPFA schemes shown in Table 1. In Fig. 8, the results show a good convergence of the numerical solutions. Here, we demonstrate again that the MPFA-O

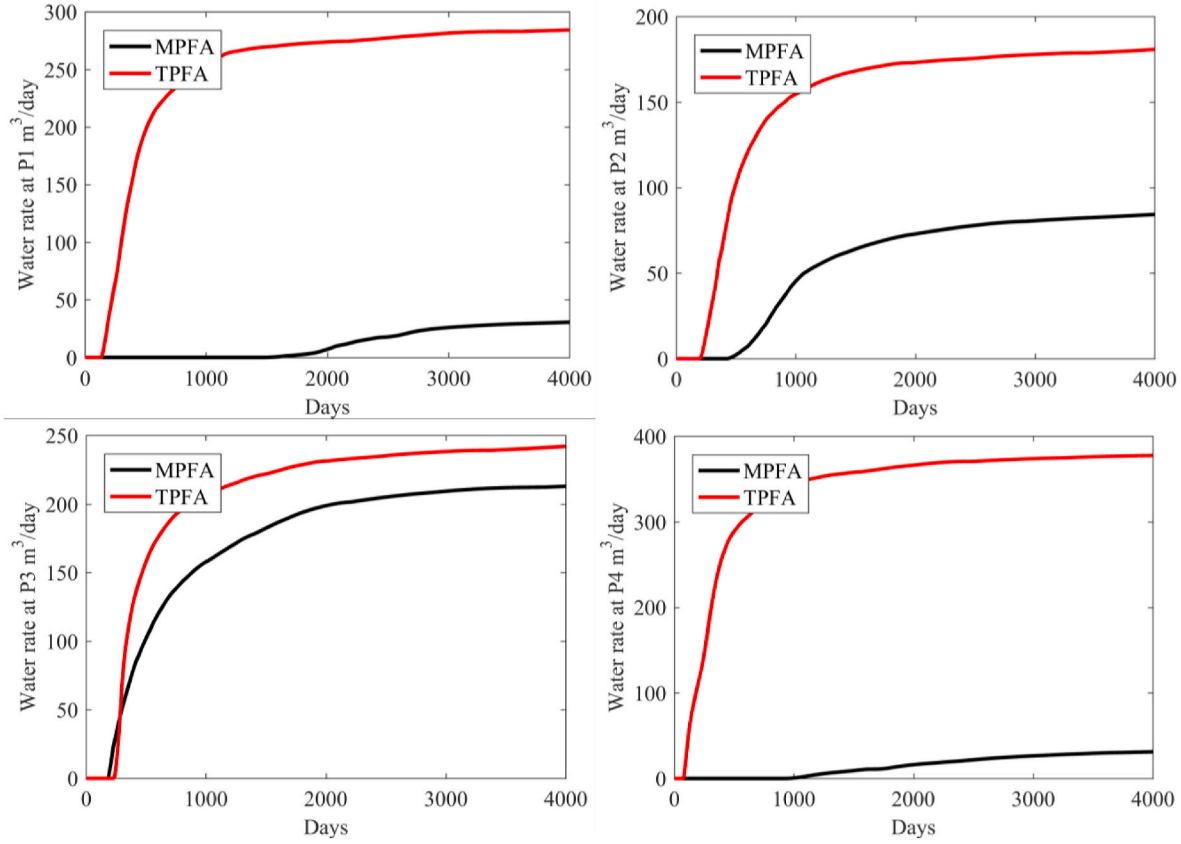

Fig. 24. Case 2 water production rate of production wells.

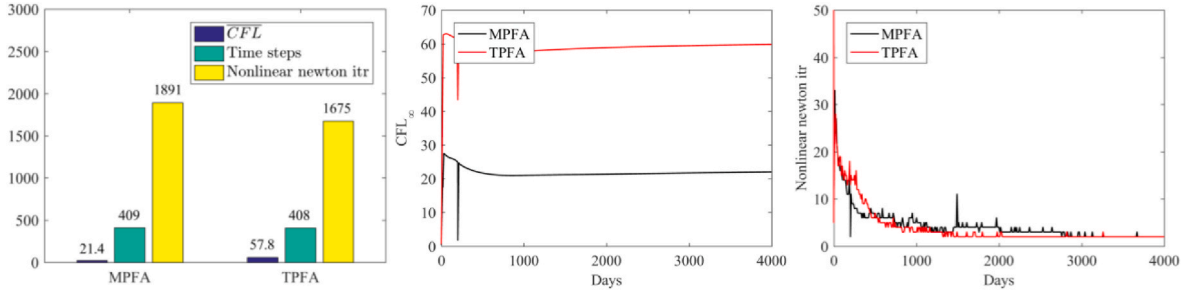

Fig. 25. Case 2 computational results of MPFA-O and TPFA schemes.

method provides the same solution with TPFA method for the simulation cases holding heterogeneities, structured grid, and diagonal permeability tensor.

3.1.2. *Unstructured grid*

Next, we test this case with an unstructured grid to further investigate the performance of the framework. For this purpose, we split each hexahedral grid into six tetrahedron grids shown in Fig. 9. By running simulations with different grid resolutions, we obtain the $L^P_{\infty-integ}$ and $L^P_{2-integ}$ shown in Table 2. In Fig. 10, we compare the solution of MPFA-O to that of TPFA scheme. It shows that the numerical errors of MPFA-O reduce with the increase of grid resolution, whereas the TPFA fails. Moreover, by observing the errors and rates of convergence of MPFA-O in Tables 1 and 2, we find that the degeneration of grid quality lowers the rate of convergence of MPFA-O. Considering the failure of TPFA in addition, the unstructured grid is only recommended for diagonal permeability cases when it is required to depict important geological features.

3.2. *Single-phase flow with full tensor permeability*

In this section, we test the framework with a full tensor permeability case. The heterogeneity and full tensor permeability in a uniform cube $[0, 1]^3$ is described in Equation (38):

$$\mathrm{K}(x,y,z) = \begin{bmatrix} y^2+z^2+1 & xy & xz \\ xy & x^2+z^2+1 & yz \\ xz & yz & x^2+y^2+1 \end{bmatrix}. \tag{38}$$

The magnitude of the full tensor permeability for the domain is shown in Fig. 11a. The analytical solution (Lipnikov et al., 2006), shown in Equation (39) and Fig. 11b, is taken as a reference for a single-phase transient flow problem.

$$P_a = \left[x^2y^3z + 3x\sin(yz)\right]e^{-t}. \tag{39}$$

Again, we will test this case with both structured and unstructured grids to study the performance of the framework.

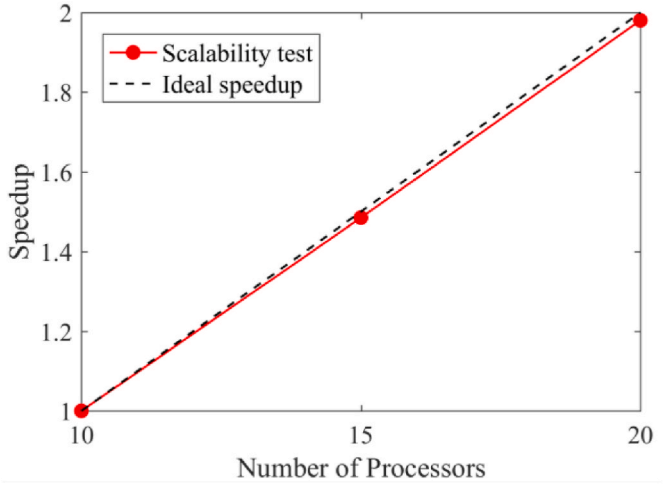

Fig. 26. Scalability of the parallel framework (normalized to 10 processors).

3.2.1. Structured grid

We obtain the numerical errors shown in Table 3 by running simulations with simulation time (5 days) and time step (0.1 days) on different structured-grid resolutions. In Fig. 12, we compare the solution of MPFA-O to that of TPFA. It shows that the solutions of MPFA-O converge to the real solution with grid refinement. The results demonstrate that MPFA-O is capable to provide convergent numerical solutions for both full tensor and diagonal permeability cases that apply a structured grid. The fact that TPFA fails to converge proves it can not handle the full tensor permeability. In addition, the big errors introduced by TPFA indicates that this discretization scheme is only recommended for the cases having diagonal permeability tensor and structured grid.

3.2.2. Unstructured grid

For further investigation, we test the previous case employing the unstructured grid. The errors and rates of convergence are shown in Table 4. Comparing the results in Tables 1–4, we find that the numerical solutions of MPFA-O holding full permeability tensor in the unstructured grid have a higher rate of convergence than that of holding diagonal permeability tensor in the unstructured grid when the rates of convergence in the structured grid are very close. An explanation for that is the multi-directional normals on the faces of unstructured grid, introduced by the degeneration of grid quality, hold higher potential to capture the diffusion in full permeability tensor cases than that of in diagonal permeability tensor cases.

In Fig. 13, we compare the solution of MPFA-O to that of TPFA. It shows that the numerical errors of MPFA-O reduce with grid refinement, whereas TPFA fails. We can conclude that the MPFA-O is capable to handle the diagonal and full permeability tensors in structured and unstructured grids. Thus, we strongly recommend it for the simulations that have a complex structure of the geological model and require a full tensor representation of permeability.

3.3. Multiphase flow with different OBL resolutions

Since the OBL is an approximation approach in essence, we need to rigorously demonstrate the accuracy of the numerical solutions in modelling multiphase flow. For this purpose, taking the Buckley-Leverett analytical solution as a reference, we investigate the convergence of numerical solutions with respect to the OBL resolution. In this test, the reservoir size is 10 × 1 × 1 m, the rock and fluid are incompressible, the reservoir is initially saturated with oil, an injection well and a production well are separately set on the left and right sides of the domain, the well rates are both fixed as 0.001 m^3/day, the simulation time is 1000 days, the domain is meshed with the hexahedral grid using dimension 10,000 × 1 × 1, the other parameters are shown in Table 5.

We run the simulation using different OBL resolutions. The numerical errors between the solutions of OBL method and traditional method (straightforward hand-differentiation), shown in Table 6 and Fig. 14, indicate that the OBL resolution affects the simulation accuracy greatly. However, with the increase of OBL resolution, the numerical solution approaches the solution of traditional method fast. In addition, we find that the OBL resolution has an influence on the CFL criteria defined in Equation (40) as well as the nonlinear newton iterations. We would like to point it out that the optimal OBL resolution for practical simulations is dependent on the degree of nonlinearity of the system.

$$CFL_\infty = \max(CFL_i),\ = \frac{\sum CFL_\infty}{\underset{\text{steps}}{\text{Time}}},\ CFL_{\infty\max} = \max(CFL_\infty), \tag{40}$$

where

$$CFL_i = \max\left(CFL_{i,in,g}, CFL_{i,in,o}, CFL_{i,in,w}, CFL_{i,out,g}, CFL_{i,out,o}, CFL_{i,out,w}\right), \tag{41}$$

$$CFL_{i,d,g} = \left|\frac{\Delta t\sum_l\left[\left(\lambda_g^l\rho_g^l + \lambda_o^l\frac{\rho_{gsc}}{B_o^l}R_g^l\right)\mathrm{T}_{integ}^l\mathrm{P}_{integ}^l\right]}{V\varphi\left(\rho_g S_g + \frac{\rho_{gsc}}{B_o}R_g S_o\right)}\right|, \begin{cases} d = in, \mathrm{T}_{integ}^l\mathrm{P}_{integ}^l \geq 0 \\ d = out, \mathrm{T}_{integ}^l\mathrm{P}_{integ}^l < 0 \end{cases}, \tag{42}$$

$$CFL_{i,d,o} = \left|\frac{\Delta t\sum_l\left(\lambda_o^l\rho_o^l\mathrm{T}_{integ}^l\mathrm{P}_{integ}^l\right)}{V\varphi\rho_o S_o}\right|, \begin{cases} d = in, \mathrm{T}_{integ}^l\mathrm{P}_{integ}^l \geq 0 \\ d = out, \mathrm{T}_{integ}^l\mathrm{P}_{integ}^l < 0 \end{cases}, \tag{43}$$

$$CFL_{i,d,w} = \left|\frac{\Delta t\sum_l\left(\lambda_w^l\rho_w^l\mathrm{T}_{integ}^l\mathrm{P}_{integ}^l\right)}{V\varphi\rho_w S_w}\right|, \begin{cases} d = in, \mathrm{T}_{integ}^l\mathrm{P}_{integ}^l \geq 0 \\ d = out, \mathrm{T}_{integ}^l\mathrm{P}_{integ}^l < 0 \end{cases}. \tag{44}$$

Here, subscript i is the index of grid block; subscript d represents the flow direction where *in* and *out* mean flowing in and flowing out the ith grid block respectively; subscript l represents all the faces of the ith grid block.

To display the simulation accuracy in an intuitive way, we show the profiles of water saturation in Fig. 15. It is clear that the numerical solution approaches the analytical solution at different simulation time which further demonstrates the accuracy of the OBL method.

3.4. Discussion

We presented several benchmark cases to demonstrate the accuracy, convergence, and robustness of the framework. For single-phase transient flow problem, we benchmarked the numerical solutions with analytical solutions applying diagonal and full permeability tensor in structured and unstructured grids. The results prove that the MPFA-O scheme could provide convergent solutions for all the tested cases when TPFA scheme only succeeds in diagonal permeability tensor case using structured grid. For multi-phase flow problems, we benchmarked the numerical solutions with the Buckley-Leverett analytical solutions. The results demonstrate that the numerical solution approaches the solution of traditional method with the refinement of OBL resolution.

We can conclude that the framework is capable to provide convergent and robust solutions for muli-phase flow problems.

4. Application cases

In this section, we present two challenging field-scale cases to further demonstrate the performance the parallel framework. First, we test a dead oil model with a bent SPE10 model using unstructured grid; second, we test a black oil model with a refined egg model holding full tensor permeability.

4.1. Case 1

We test a dead oil model with the full layers of SPE10 model of which a large gridblock number (1.122 million) and various permeability contrast introduce a great challenge for reservoir simulation. Moreover, to prove the modelling capabilities of MPFA-O, we bend the geological model to generate an unstructured domain that is shown in Fig. 16. The initial pressure is 300 bar, the rock and fluid are incompressible, the viscosities of water and oil are equalling to 1 and 2 cP respectively, the initial water saturation is 0.2, the relative permeability model is defined as $k_{rw} = [(S_w\text{-}S_{wc})/(1\text{-}S_{wc}\text{-}S_{or})]^2$ and $k_{ro} = [(S_o\text{-}S_{or})/(1\text{-}S_{wc}\text{-}S_{or})]^2$ where $S_{wc} = 0.2$ and $S_{or} = 0.2$. We set an injection well in the middle of the geological model and four production wells at the corners (Fig. 17). The locations of the four producers are (2, 1.5), (2, 658.5), (238, 658.5), and (238, 1.5) respectively. The bottom hole pressures of injector and producers are equalling to 350 and 250 bar respectively. The OBL resolution is 128, the simulation time is 2000 days with a maximum time step of 20 days.

After domain decomposition, the bent SPE10 model is divided into 48 subdomains that are shown in Fig. 17. Note that a well should be fully inside a single subdomain. Fig. 18 shows the pressure and water saturation distributions of MPFA-O and TPFA schemes. We can see an obvious difference in the pressure solution which indicates the TPFA fails to capture the flow response in unstructured domain. Moreover, the failure of honoring grid orthogonality makes it hard for TPFA scheme to predict the pathway of the injected water.

To quantify the error of TPFA in water saturation that is a vital indicator for the evaluation of water flooding strategy, we show the water cut of production wells in Fig. 19. We can find that the water breakthrough time of TPFA scheme is earlier than that of MPFA scheme. This difference could significantly affect the results of development strategy selection and uncertainty quantification.

Fig. 20 shows the CFL, time steps, and nonlinear newton iterations of MPFA-O and TPFA schemes. We can find that the CFL of TPFA is much larger than that of MPFA-O. The explanation for the difference is that the water flows faster in TPFA scheme which is intuitively shown in the water saturation distributions in Fig. 18. Moreover, the results indicate that the failure of honoring grid orthogonality changes the displacing process physically and convergent process computationally. Thus, a predictive simulation of an unstructured domain requires advancing discretization schemes such as the MPFA-O scheme.

4.2. Case 2

In this case, we test a black oil model with a refined egg model (Jansen et al., 2014). The dx, dy, and dz of the structured grid are refined as 4, 4, and 2 m respectively, the PVT properties and relative permeabilities are taken from the SPE9 test case (Killough, 1995), the porosity is 0.2, the rock compressibility is 1.450377E-5 bar^{-1}, the initial pressure is 300 bar, the mass fractions of gas, oil, and water component are 0.227, 0.588, and 0.185 respectively. We set an injection well and four producers (Fig. 22) with well locations shown in Table 7. The bottom hole pressures of injector and producers are equalling to 340 and 260 bar respectively. The OBL resolution is 128, the simulation time is 4000 days with a maximum time step equaling 10 days. The permeability distribution is shown in Fig. 21. For the purpose of testing a full tensor permeability case, we rotate the diagonal tensor as following:

$$\mathbf{K} = R_z(30^\circ)\mathrm{diag}(K_x, 0.01K_x, 0.005K_x)R_z^T(30^\circ), R_z(\theta) = \begin{bmatrix} cos(\theta) & sin(\theta) & 0 \\ -sin(\theta) & cos(\theta) & 0 \\ 0 & 0 & 1 \end{bmatrix}. \tag{45}$$

Fig. 22 shows the result of the domain decomposition of the egg model with 20 subdomains. Fig. 23 shows the pressure and water saturation distributions. We find that the rotated permeability tensor imposes an obvious constraint on the pressure distribution of MPFA-O scheme but barely affects that of TPFA scheme. Moreover, the difference in honoring grid orthogonality makes the two schemes turn out an obviously different water saturation distribution. We quantify this difference in Fig. 24 which shows earlier water breakthrough in P1, P2, and P4 for the TPFA scheme. The results demonstrate that it is difficult for the TPFA scheme to provide reliable solutions for full tensor permeability cases as well.

Fig. 25 shows the CFL, time steps, and nonlinear newton iterations of MPFA-O and TPFA schemes. Because of the modification of displacing process, the TPFA scheme provides a higher CFL_∞ than that of MPFA-O scheme.

Finally, we test the scalability of the framework by running the simulation with different numbers of processors. Fig. 26 shows the speedup versus the number of processors. The results demonstrate strong scalability of the parallel framework for reservoir simulation.

4.3. Discussion

We investigated the performance of the new parallel framework with two applied challenging cases. In the first case, we bent the domain of SPE10 model to show the capabilities of handling unstructured grid. The simulation results indicate that the TPFA scheme introduces large numerical errors in field-scale unstructured-domain case. We also quantified the computational results by measuring the water breakthrough, CFL, time steps, and nonlinear newton iterations of MPFA-O and TPFA schemes. In the second case, we rotated the permeability tensor of a refined egg model to demonstrate the modelling capabilities for full tensor permeability case. The distinctive difference in pressure distributions indicates that the TPFA scheme can not reproduce the expected flow response within the constraints imposed by permeability tensor. Because of that, the water saturation distribution and water breakthrough time differ greatly between the solutions for the two schemes. The scalability test proves a good parallel performance of the framework.

5. Conclusions

In this work, we applied Message Passing Interface for MPFA-O scheme with state-of-the-art Operator-Based Linearization (OBL) approach for fluid flow in porous media. Although the MPFA-O scheme may have some trouble to get the invesrse of A in equation (19) for highly distorted meshes and/or highly anisotropic media, most of the geological models used for reservoir simulation match its requirement on mesh quality and anisotropy. Thus, as the MPFA-O scheme could handle non-**K**-orthogonal mesh and is implemented on a general unstructured grid, the reservoir simulator is powerful to simulate complex cases that have unstructured domain and full tensor permeability.

To keep the extensibility of the framework, we used the operator-based representation of governing equations and the mass-based formulation to describe the physical processes in oil and gas field development. Benefit from that, the governing equations of single-phase, two-phase dead oil, three-phase black oil, and compositional models can be unified. However, the state-dependent operators could introduce Jacobian assembly hassle and potentially large computation time of complex phase behavior evaluation since we applied the fully implicit scheme that is unconditionally stable to solve the nonlinear

system. To deal with that, we applied the OBL that uniformly discretizes the parameter space of the unknowns. Based on that, a tabulated representation of physics can be constructed by computing the values of operators on vertices of hypercubes. Accordingly, the operator values and their derivatives, required by the residual and Jacobian assembly, can be determined by multi-linear interpolation. In this way, the programming complexity or Jacobian assembly for complex physical problems is drastically simplified.

In order to simulate results at a geological scale, we used massively parallel computations via Message Passing Interface (MPI) to improve the computational efficiency. The construction of shared and ghost cells for MPFA-O scheme is more complicated than that for the traditional TPFA scheme. To demonstrate the performance of the framework, we presented several benchmark cases and field-scale cases. First, we benchmarked the numerical solutions with analytical solutions for single-phase flow. The results show that the framework is capable to provide convergent solutions for heterogeneous cases holding full/diagonal permeability tensor in a structured/unstructured grid. Second, we compared the numerical solutions to Buckley-Leverett analytical solutions for two-phase flow which rigorously demonstrates the robustness and accuracy of the OBL method. Finally, we tested two challenging field-scale cases holding high heterogeneities, large grid-block numbers, unstructured gridding, and full tensor permeability. The results show advanced modelling capabilities and parallel scalability for complex reservoir simulations.

We demonstrated that a combination of the OBL and MPFA can guarantee accurate solutions for complex cases with strong heterogeneity, unstructured grid, and full tensor permeability. To enhance the simulation capabilities for highly distorted meshes and/or highly anisotropic media, we will include the monotone nonlinear finite-volume schemes and non-classic MPFA schemes with good robustness and accuracy in our simulator.

Author contribution

Longlong Li: Methodology, Software, Investigation, Writing – original draft, Writing - Review & Editing. Mark Khait: Software. Denis Voskov: Software. Kirill M. Terekhov: Software. Ahmad Abushaikha: Methodology, Writing – original draft, Funding acquisition.

Declaration of competing interest

The authors declare that they have no known competing financial interests or personal relationships that could have appeared to influence the work reported in this paper.

Data availability

Data will be made available on request.

Acknowledgments

This publication was supported by the National Priorities Research Program grant NPRP10-0208-170407 from Qatar National Research Fund.

References

Aavatsmark, I., 2007. Multipoint flux approximation methods for quadrilateral grids. In: 9th International Forum on Reservoir Simulation. Abu Dhabi.
Aavatsmark, I., Eigestad, G.T., 2006. Numerical convergence of the MPFA Omethod and U-method for general quadrilateral grids. Int. J. Numer. Methods Fluid. 51, 939–961.
Aavatsmark, I., Barkve, T., Bøe, Ø., Mannseth, T., 1994. Discretization on non-orthogonal, curvilinear grids for multi-phase flow. In: Proceedings of the Fourth European Conference on the Mathematics of Oil Recovery. Røros, Norway.
Aavatsmark, I., Barkve, T., Bøe, Ø., Mannseth, T., 1996a. Discretization on non-orthogonal, quadrilateral grids for inhomogeneous, anisotropic media. J. Comput. Phys. 127, 2–14.
Aavatsmark, I., Barkve, T., Bøe, Ø., Mannseth, T., 1996b. A class of discretization methods for structured and unstructured grids in anisotropic, inhomogeneous media. In: Proceedings of 5th European Conference on the Mathematics of Oil Recovery. Leoben, Austria.
Aavatsmark, I., Barkve, T., Mannseth, T., 1998. Control-volume discretization methods for 3D quadrilateral grids in inhomogeneous, anisotropic reservoirs. SPE J. 3, 146–154.
Aavatsmark, I., Eigestad, G.T., Klausen, R.A., 2006. Numerical convergence of the MPFA O-method for general quadrilateral grids in two and three dimensions. In: Arnold, D. N., Bochev, P.B., Lehoucq, R.B., Nicolaides, R.A., Shashkov, M. (Eds.), Compatible Spatial Discretizations, Volume 142 of IMA Vol. Math. Appl. Springer, New York, pp. 1–21.
Aavatsmark, I., Eigestad, G.T., Klausen, R.A., Wheeler, M.F., Yotov, I., 2007a. Convergence of a symmetric MPFA method on quadrilateral grids. Comput. Geosci. 11, 333–345.
Aavatsmark, I., Eigestad, G.T., Heimsund, B.-O., Mallison, B.T., Nordbotten, J.M., Øian, E., 2007b. A new finite volume approach to efficient discretization on challenging grids. Houston. In: Proc. SPE Reservoir Simulation Symposium. SPE 106435.
Aavatsmark, I., Eigestad, G.T., Mallison, B.T., Nordbotten, J.M., 2008. A compact multipoint flux approximation method with improved robustness. Numer. Methods Part. Differ. Equ. 24 (5), 1329–1360.
Abhyankar, S., Adams, M.F., et al., 2014. PETSc Web Page.
Abushaikha, A.S., Terekhov, K.M., 2020. A fully implicit mimetic finite difference scheme for general purpose subsurface reservoir simulation with full tensor permeability. J. Comput. Phys., 109194
Abushaikha, A.S., Blunt, M.J., Gosselin, O.R., Pain, C.C., Jackson, M.D., 2015. Interface control volume finite element method for modelling multi-phase fluid flow in highly heterogeneous and fractured reservoirs. J. Comput. Phys. 298, 41–61.
Abushaikha, A.S., Voskov, D.V., Tchelepi, H.A., 2017. Fully implicit mixed-hybrid finite-element discretization for general purpose subsurface reservoir simulation. J. Comput. Phys. 346, 514–538.
Alpak, F.O., 2010. A mimetic finite volume discretization method for reservoir simulation. SPE J. 15 (2), 436–453.
Arrarás, A., Portero, L., 2019. Multipoint flux mixed finite element methods for slightly compressible flow in porous media. Comput. Math. Appl. 77 (6), 1437–1452.
Aziz, K., Settari, A., 1979. Petroleum Reservoir Simulation. Chapman & Hall.
Brezzi, F., Fortin, M., 1991. Mixed and Hybrid Finite Element Methods. Springer, Berlin.
Cao, H., 2002. Development of Techniques for General Purpose Simulators. Stanford University, United States.
Cao, Y., Helmig, R., Wohlmuth, B., 2009. Geometrical interpretation of the multi-point flux approximation l-method. Int. J. Numer. Methods Fluid. 60 (11), 1173–1199.
Contreras, F.R.L., Lyra, P.R.M., de Carvalho, D.K.E., 2019. A new multipoint flux approximation method with a quasi-local stencil (MPFA-QL) for the simulation of diffusion problems in anisotropic and heterogeneous media. Appl. Math. Model. 70, 659–676.
Edwards, M.G., Rogers, C.F., 1994. A flux continuous scheme for the full tensor pressure equation. In: Proceedings of the Fourth European Conference on the Mathematics of Oil Recovery. Røros.
Edwards, M.G., Rogers, C.F., 1998. Finite volume discretization with imposed flux continuity for the general tensor pressure equation. Comput. Geosci. 2 (4), 259–290.
Eigestad, G.T., Klausen, R.A., 2005. On the convergence of the multi-point flux approximation O-method: numerical experiments for discontinuous permeability. Numer. Methods Part. Differ. Equ. 21, 1079–1098.
Faille, I., 1992. A control volume method to solve an elliptic equation on a twodimensional irregular mesh. Comput. Methods Appl. Mech. Engrg. 100, 275–290.
Forsyth, P.A., Sammon, P.H., 1988. Quadratic convergence for cell-centered grids. Appl. Numer. Math. 4, 377–394.
Gao, Z., Wu, J., 2013. A small stencil and extremum-preserving scheme for anisotropic diffusion problems on arbitrary 2D and 3D meshes. J. Comput. Phys. 250, 308–331.
Garipov, T.T., Karimi-Fard, M., Tchelepi, H.A., 2016. Discrete fracture model for coupled flow and geomechanics. Comput. Geosci. 20 (1), 149–160.
Garipov, T.T., Tomin, P., Rin, R., Voskov, D.V., Tchelepi, H.A., 2018. Unified thermo-compositional-mechanical framework for reservoir simulation. Comput. Geosci. 22 (4), 1039–1057.
Jansen, J.D., Fonseca, R.M., Kahrobaei, S., et al., 2014. The egg model: a geological ensemble for reservoir simulation. Geosci. Data J. 1, 192–195.
Khait, M., Voskov, D.V., 2016. Operator-based linearization for non-isothermal multiphase compositional flow in porous media. In: 15th European Conference on the Mathematics of Oil Recovery. ECMOR.
Khait, M., Voskov, D.V., 2017. Operator-based linearization for general purpose reservoir simulation. J. Petrol. Sci. Eng. 157, 990–998.
Khait, M., Voskov, D.V., 2018a. Operator-based linearization for efficient modeling of geothermal processes. Geothermics 74, 7–18.
Khait, M., Voskov, D.V., 2018b. Adaptive parameterization for solving of thermal/compositional nonlinear flow and transport with buoyancy. SPE J. 23 (2).
Killough, J.E., 1995. Ninth SPE comparative solution project: a reexamination of black-oil simulation. San Antonio, Texas. In: SPE Reservoir Simulation Symposium. SPE-29110-MS.
Klausen, R.A., Winther, R., 2006a. Convergence of multipoint flux approximations on quadrilateral grids. Numer. Methods Part. Differ. Equ. 22, 1438–1454.
Klausen, R.A., Winther, R., 2006b. Robust convergence of multi point flux approximation on rough grids. Numer. Math. 104, 317–337.

Li, L., Abushaikha, A., 2020. An advanced parallel framework for reservoir simulation with mimetic finite difference discretization and operator-based linearization. In: ECMOR XVII-17th European Conference on the Mathematics of Oil Recovery.
Li, L., Abushaikha, A., 2022. A fully-implicit parallel framework for complex reservoir simulation with mimetic finite difference discretization and operator-based linearization. Comput. Geosci. 26, 915–931.
Li, B., Chen, Z., Huan, G., 2004. Comparison of solution schemes for black oil reservoir simulations with unstructured grids. Comput. Methods Appl. Mech. Eng. 193, 319–355.
Li, L., Khait, M., Voskov, D.V., Abushaikha, A.S., 2020. Parallel framework for complex reservoir simulation with advanced discretization and linearization schemes. Amsterdam, Netherlands. In: The SPE Europec Featured at 82nd EAGE Conference and Exhibition. SPE-200615-MS.
Lie, K.-A., Krogstad, S., Ligaarden, I.S., Natvig, J.R., Nilsen, H.M., Skaflestad, B., 2012. Open-source matlab implementation of consistent discretisations on complex grids. Comput. Geosci. 16 (2), 297–322.
Lipnikov, K., Shashkov, M., Svyatskiy, D., 2006. The mimetic finite difference discretization of diffusion problem on unstructured polyhedral meshes. J. Comput. Phys. 211, 473–491.
Lipnikov, K., Manzini, G., Shashkov, M., 2014. Mimetic finite difference method. J. Comput. Phys. 257, 1163–1227.
Moortgat, J., Firoozabadi, A., 2016. Mixed-hybrid and vertex-discontinuous-Galerkinfinite element modeling of multiphase compositional flow on 3Dunstructured grids. J. Comput. Phys. 315, 476–500.
Moshiri, M., Manzari, M.T., 2019. Simulation of multi-component multi-phase fluid flow in two-dimensional anisotropic heterogeneous porous media using high-order control volume distributed methods. Comput. Math. Appl. 78 (10), 3303–3328.
Njifenjou, A., Nguena, I.M., 2006. A finite volume approximation for second order elliptic problems with a full matrix on quadrilateral grids: derivation of the scheme and a theoretical analysis. Int. J. Finite 3.
Nordbotten, J.M., Eigestad, G.T., 2005. Discretization on quadrilateral grids with improved monotonicity properties. J. Comput. Phys. 203 (2), 744–760.
Pal, M., Edwards, M.G., Lamb, A.R., 2006. Convergence study of a family of flux-continuous, finite-volume schemes for the general tensor pressure equation. Int. J. Numer. Methods Fluid. 51, 1177–1203.
Pruess, K., 2004. The TOUGH codes–A family of simulation tools for multiphase flow and transport processes in permeable media. Vadose Zone J. 3 (3), 738–746.
Pruess, K., Oldenburg, C.M., Moridis, G., 1999. TOUGH2 User's Guide, Version 2.0. Report LBNL-43134. Lawrence Berkeley National Laboratory, Berkeley, CA, USA.
Schneider, M., Flemisch, B., Helmig, R., et al., 2018. Monotone nonlinear finite-volume method for challenging grids. Comput. Geosci. 22 (2), 565–586.
Settari, A., Aziz, K., 1972. Use of irregular grid in reservoir simulation. SPE J. 12 (2), 103–114.
Souza, M.R., Contreras, F.R., Lyra, P.R., et al., 2018. A higher-resolution flow-oriented scheme with an adaptive correction strategy for distorted meshes coupled with a robust MPFA-D method for the numerical simulation of two-phase flow in heterogeneous and anisotropic petroleum reservoirs. SPE J. 23 (6), 2351–2375.
Terekhov, K.M., Mallison, B.T., Tchelepi, H.A., 2017. Cell-centered nonlinear finite-volume methods for the heterogeneous anisotropic diffusion problem. J. Comput. Phys. 330, 245–267.
Terekhov, K.M., Vassilevski, Y., 2019. INMOST parallel platform for mathematical modeling and applications. In: Voevodin, V., Sobolev, S. (Eds.), Supercomputing. RuSCDays 2018. Communications in Computer and Information Science 965. Springer, Cham.
Tikhonov, A.N., Samarskii, A.A., 1962. Homogeneous difference schemes. Comput. Math. Math. Phys. 1 (1), 5–67.
Van der Vorst, H.A., 1992. Bi-CGSTAB: a fast and smoothly converging variant of Bi-cg for the solution of nonsymmetric linear systems. SIAM J. Sci. Stat. Comput. 13, 631–644.
Voskov, D.V., 2012. An extended natural variable formulation for compositional simulation based on tie-line parameterization. Transport Porous Media 92 (3), 541–557.
Voskov, D.V., 2017. Operator-based linearization approach for modeling of multiphase multi-component flow in porous media. J. Comput. Phys. 337, 275–288.
Wang, Y., Voskov, D.V., Khait, M., Bruhn, D., 2020. An efficient numerical simulator for geothermal simulation: a benchmark study. Appl. Energy 264, 114693.
Wheeler, M.F., Yotov, I., 2006. A multipoint flux mixed finite element method. SIAM J. Numer. Anal. 44 (5), 2082–2106.
Younes, A., Fontaine, V., 2008. Efficiency of mixed hybrid finite element and multipoint flux approximation methods on quadrangular grids and highly anisotropic media. Int. J. Numer. Methods Eng. 76 (3), 314–336.
Zaydullin, R., Voskov, D.V., James, S.C., Henley, H., Lucia, A., 2014. Fully compositional and thermal reservoir simulation. Comput. Chem. Eng. 63, 51–65.
Zhang, Q., Huang, Z., Yao, J., Wang, Y., Li, Y., 2017. Multiscale mimetic method for two-phase flow in fractured media using embedded discrete fracture model. Adv. Water Resour. 107, 180–190.